Journal of Instrumentation

SISSA

PAPER • OPEN ACCESS

Beam physics research with the IOTA electron lens

To cite this article: G. Stancari *et al* 2021 *JINST* **16** P05002

Published by IOP Publishing for Sissa Medialab

Received: *April 13, 2021*
Accepted: *April 26, 2021*
Published: *May 3, 2021*

ICFA Beam Dynamics Newsletter#81 —
Electron Lenses for Modern and Future Accelerators

Beam physics research with the IOTA electron lens

G. Stancari,[a,*] R. Agustsson,[f] N. Banerjee,[c] C. Boffo,[a] A. Burov,[a] K. Carlson,[a] B. Cathey,[a] Y.-C. Chen,[f] M. Chung,[h] D. Crawford,[a] R. Dhuley,[a] N. Eddy,[a] B. Freemire,[d] C. Hall,[g] Y.-K. Kim,[c] A. Kolehmainen,[b] V. Lebedev,[a] A. Murokh,[f] S. Nagaitsev,[a,c] C.S. Park,[e] D. Perini,[b] A. Romanov,[a] J. Ruan,[a] V. Shiltsev,[a] A. Smirnov,[f] E. Stern[a] and A. Valishev[a]

[a] *Fermi National Accelerator Laboratory, Batavia, Illinois 60510, U.S.A.*
[b] *CERN, European Organization for Nuclear Research, CH-1211 Geneva 23, Switzerland*
[c] *The University of Chicago, Chicago, Illinois 60637, U.S.A.*
[d] *Euclid Techlabs, Bolingbrook, Illinois 60440, U.S.A.*
[e] *Korea University, Sejong 30019, South Korea*
[f] *RadiaBeam Technologies, Santa Monica, California 90404, U.S.A.*
[g] *RadiaSoft, Boulder, Colorado 80301, U.S.A.*
[h] *Ulsan National Institute of Science and Technology, Ulsan 44919, South Korea*

E-mail: stancari@fnal.gov

Abstract: The electron lens in the Fermilab Integrable Optics Test Accelerator (IOTA) will enable new research in nonlinear integrable optics, space-charge compensation, electron cooling, and the stability of intense beams. This research addresses scientific questions on high-brightness beams and operational challenges of high-power accelerators for nuclear and particle physics. We review the roles that electron lenses play in this field and the physical principles behind their applications. The design criteria and specifications for the IOTA storage ring and electron lens are then discussed. We conclude with a description of the components of the apparatus.

Keywords: Accelerator modelling and simulations (multi-particle dynamics; single-particle dynamics); Accelerator Subsystems and Technologies; Beam dynamics

*Corresponding author.

https://doi.org/10.1088/1748-0221/16/05/P05002

2021 JINST 16 P05002

Contents

2021 JINST 16 P05002

1 Electron lenses and the IOTA research program

In the Fermilab Integrable Optics Test Accelerator (IOTA) [1], a rich beam physics research program has started. Part of this program is based on novel applications of electron lenses. After an introduction on electron lenses and on the IOTA ring, we outline the scientific program, describe the experimental design criteria, and give an overview of the apparatus.

1.1 The IOTA storage ring and beam physics program

IOTA is a storage ring dedicated to beam physics research (figure 1). It can operate with both electrons or protons and it is part of the Fermilab Accelerator Science and Technology (FAST) facility [1], which also includes the FAST superconducting linac. The IOTA/FAST complex has three main purposes: (i) to address the challenges posed by future high-intensity machines, such as instabilities and losses; (ii) to carry out basic research in beam physics; and (iii) to provide education and training for scientists and engineers.

IOTA is unique also because of its flexibility. It has a circumference of 40 m and a relatively large aperture diameter (50 mm). It can be reconfigured to accommodate different experiments and, because of the quality of the instrumentation, the magnetic lattice can be precisely controlled. In addition, the lattice itself was designed to have significant flexibility to enable a wide variety of studies. IOTA can store electrons up to a kinetic energy of 150 MeV or protons at 2.5 MeV. The main IOTA parameters are listed in table 1. Because of the relatively fast synchrotron-radiation damping and small equilibrium emittances, electrons are ideal for the study of linear and nonlinear single-particle effects. With protons, on the other hand, very large space-charge tune shifts $\Delta\nu_{sc}$ are achievable. Many fundamental questions on the physics of high-brightness beams can be studied, such as the effect of nonlinear integrable lattices on instability thresholds, the interplay between space charge and nonlinearities, space-charge compensation, emittance evolution, halo formation and beam diagnostics.

One of the pillars of the IOTA research program is the experimental study of nonlinear integrable focusing systems [2–11]. Because of their nonlinearity, these systems generate a betatron tune spread, protecting the beam from instabilities through Landau damping. Integrability ensures that the nonlinearity does not reduce the dynamic aperture of the machine, thus preserving beam lifetime and emittance. The experimental demonstration of these concepts can significantly impact the design and performance of high-intensity accelerators for nuclear and particle physics. Several other topics are being studied in IOTA, such as the statistical properties of undulator radiation [12–14] and the experimental demonstration of optical stochastic cooling [15]. In addition, IOTA has the capability of storing single electrons or a small known number of electrons [16, 17]. Experiments on the coherence properties of two-photon undulator radiation from a single electron, for instance, will take place in the near future.

Electrons were circulated in IOTA for the first time in August 2018. Typically, the machine runs for a few months, after which it is shut down for maintenance and upgrades and reconfigured for the next experimental run. IOTA Run 1 lasted until April 2019. Run 2 took place between November 2019 and March 2020. Currently, the machine is being commissioned for Run 3. Installation of the proton injector is scheduled to be completed at the end of 2021, enabling research on space-charge-dominated beams. The ability to switch between proton and electron operations

2021 JINST 16 P05002

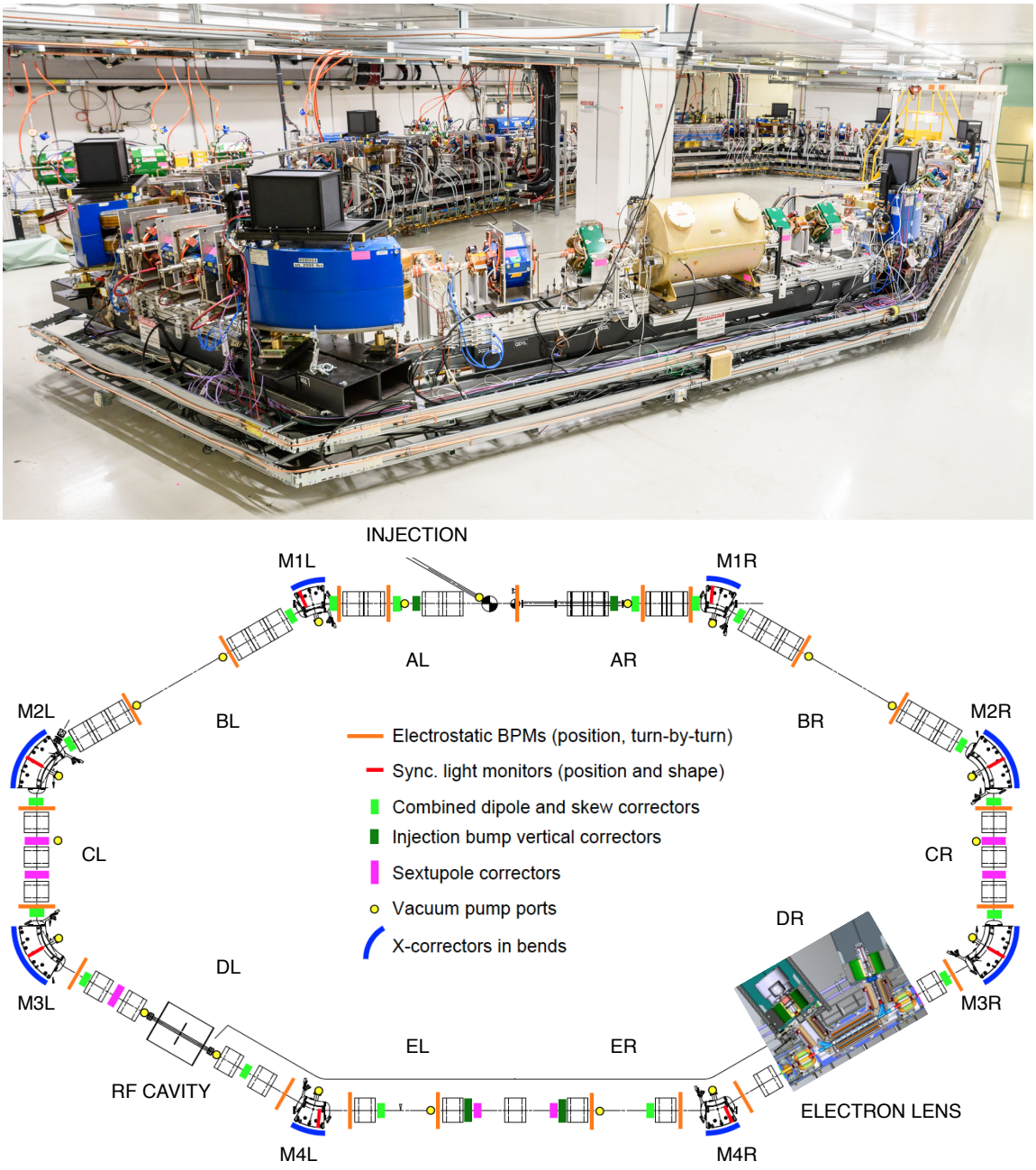

Figure 1. The IOTA storage ring at Fermilab. The layout shows the planned location of the electron lens. The sectors are named AR (A Right), BR, etc. through AL (A Left). The dipole magnets and the corresponding synchrotron-radiation stations are labeled as M1R, M2R, . . . , M1L. (Photo: Giulio Stancari / Fermilab)

2021 JINST 16 P05002

will be maintained, both for commissioning and for physics. Installation of the IOTA electron lens is tentatively scheduled for the second half of 2022. More information on the IOTA physics program can be found on the Web page of the IOTA/FAST Scientific Committee [18].

1.2 Roles of the IOTA electron lens

Electron lenses are a flexible instrument for beam physics research and for accelerator operations. Several applications were demonstrated experimentally. They were first used in the Fermilab Tevatron collider for beam-beam compensation, abort-gap cleaning, and halo collimation [19–22]. In the Relativistic Heavy Ion Collider (RHIC) at Brookhaven National Laboratory, electron lenses allowed experiments to reach significantly higher luminosities [23]. Recently, hollow electron lenses for active halo control were included among the upgrades of the Large Hadron Collider at CERN to reach higher luminosities (HL-LHC Project) [24–30]. Future applications also include space-charge compensation in synchrotrons at FAIR [31].

The electron lens is based on low-energy, magnetically confined electron beams overlapping with the circulating beam in a straight section of a circular particle accelerator or storage ring. One of the main strengths of electron lenses is the possibility to shape the transverse profile and time structure of the electron beam to obtain the desired effect on the circulating beam through electromagnetic interactions [20, 32]. Moreover, the solenoidal magnetic field used in the overlap region enhances the stability of the two-beam system.

Research with electron lenses is an essential part of the IOTA scientific program. First of all, an electron lens can be used as a nonlinear element to create integrable lattices (section 2.1). There are at least two ways to accomplish this: (i) the McMillan lens and (ii) the axially symmetric thick lens. These studies will be carried out with circulating electrons first, then with protons. Secondly, the electron lens can act as an electron cooler to enable experiments with protons that require a range of beam lifetimes, emittances and brightnesses (section 2.2). Electron cooling

Table 1. Typical IOTA parameters for operation with electrons or protons.

	Electrons	Protons
Circumference, C	39.96 m	39.96 m
Kinetic energy, K_b	100–150 MeV	2.5 MeV
Revolution period, τ_{rev}	133 ns	1.83 µs
Revolution frequency, f_{rev}	7.50 MHz	0.547 MHz
Rf harmonic number, h	4	4
Rf frequency, f_{rf}	30.0 MHz	2.19 MHz
Max. rf voltage, V_{rf}	1 kV	1 kV
Number of bunches	1	4 or coasting
Bunch population, N_b	1 e^- – 3.3×10^9 e^-	$< 5.7 \times 10^9$ p
Beam current, I_b	1.2 pA – 4 mA	< 2 mA
Transverse emittances (rms, geom.), $\epsilon_{x,y}$	20–90 nm	3–4 µm
Momentum spread, $\delta_p = \Delta p/p$	$1–4 \times 10^{-4}$	$1–2 \times 10^{-3}$
Radiation damping times, $\tau_{x,y,z}$	0.2–2 s	–
Max. space-charge tune shift, $\lvert\Delta\nu_{\mathrm{sc}}\rvert$	$< 10^{-3}$	0.5

2021 JINST 16 P05002

has a long history, but this is the first time that cooling and lens capabilities are integrated in a single device. Another important function of electron lenses is their ability to generate tune shifts and tune spreads, tailored to each bunch train, as demonstrated in the Tevatron and at RHIC. For high-energy colliders, electron lenses are the best option to enhance the stabilizing mechanism of Landau damping (section 2.3). In IOTA, we plan to study this option further, with experimental demonstrations of the electron lens as Landau element to suppress instabilities introduced in a controlled way. Finally, the physics and technology of space-charge compensation in rings can be addressed (section 2.4). Demonstrations have been attempted in the past but were never fully achieved. For this purpose, we envisage two scenarios using the IOTA electron lens: (i) an 'electron column', where the low-energy electron beam is off, the negative compensating charge is generated by the protons via residual-gas ionization, and the secondary electrons are trapped as a non-neutral plasma column in a Penning-Malmberg configuration; or (ii) an electron lens with transverse and possibly longitudinal profiles tailored to compensate the space charge of the proton beam. These applications are described in more detail in the following sections, together with an outlook on other advanced topics. Part of this research requires circulating electrons for commissioning and to measure linear and nonlinear single-particle effects. Experiments on intensity effects and space charge will be carried out with proton beams.

In IOTA, the electron lens will be installed in the DR straight section (figure 1). The length of the section is 1.4 m. The layout of the IOTA electron lens is shown in figure 2. The low-energy electron beam (0.5–10 keV, typically) is generated in the electron gun and transported through

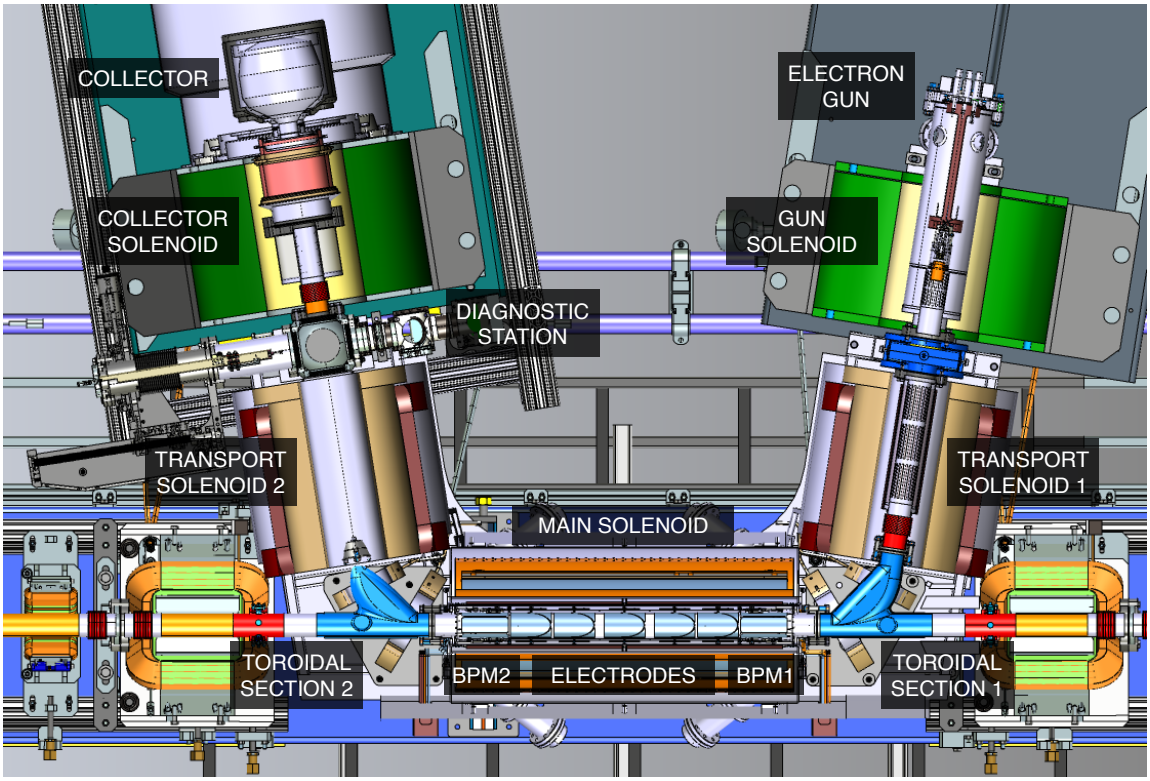

Figure 2. Layout of the IOTA electron lens.

2021 JINST 16 P05002

solenoid channels and a toroidal section to the overlap region, where it interacts with the IOTA circulating beam — electrons or protons. It is then directed towards the collector in a similar way. A summary of the IOTA electron lens parameters is given in table 2. The design criteria are discussed in more detail in section 3. Some of the main components of the apparatus are described in section 4.

The cathode-anode voltage V determines the velocity $v_e = \beta_e c$ of the electrons in the device, which has length L and is located in a region of the ring with equal lattice amplitude functions $\beta_x = \beta_y = \hat{\beta}$. When acting on a circulating beam with magnetic rigidity $(B\rho)$ and velocity $v_z = \beta_b c$, the linear focusing strength k_e for circulating particles with small betatron oscillation amplitudes is proportional to the magnitude of the electron current density on axis j_0:

$$k_e = 2\pi \frac{j_0 L(1 \pm \beta_e\beta_b)}{(B\rho)\beta_e\beta_b c^2} \left(\frac{1}{4\pi\epsilon_0}\right) \frac{q_e q_b}{|q_e q_b|}. \tag{1.1}$$

The '−' sign applies when the beams are co-propagating and the electric and magnetic forces act in opposite directions. The last term contains the charges of the electron beam q_e and of the circulating particles q_b. It indicates a focusing effect ($k_e < 0$, restoring force) or a defocusing effect ($k_e > 0$). At large electron beam currents in the electron lens, the focusing of the electron beam itself may of course distort the lattice. For small focusing strengths and away from the half-integer resonance, these kicks translate into the tune shift

$$\Delta\nu = -\frac{\hat{\beta} j_0 L(1 \pm \beta_e\beta_b)}{2(B\rho)\beta_e\beta_b c^2} \left(\frac{1}{4\pi\epsilon_0}\right) \frac{q_e q_b}{|q_e q_b|}. \tag{1.2}$$

for particles circulating near the axis. Different current-density distributions $j(r)$ introduce a radial dependence in the focusing strength and therefore different linear or nonlinear effects on the

Table 2. Typical IOTA electron lens parameters.

Parameter	Value
Lattice amplitude functions, $\hat{\beta}$	2–4 m
Circulating beam size (rms), e^-	0.4–0.6 mm
Circulating beam size (rms), p	0.9–4 mm
Circulating beam divergence (rms), e^-	0.15–0.21 mrad
Circulating beam divergence (rms), p	0.3–1.4 mrad
Cathode-anode voltage, V	0.5–10 kV
Peak current, I_e	5 mA – 3 A
Pulse width	200 ns to DC
Pulse repetition rate	DC to 10 kHz
Cathode radius, r_c	< 15 mm
Current-density distributions	McMillan, Gaussian, flat, semi-hollow
Length of the main solenoid, L	0.7 m
Main solenoid field, B_m	0.1–0.5 T
Gun and collector solenoid fields, B_g and B_c	0.1–0.4 T
Beam size compression, $\sqrt{B_m/B_g}$	0.5–2.2
Current-density magnification, B_m/B_g	0.25–5

2021 JINST 16 P05002

circulating beam. The time structure of the low-energy electron pulse can also be varied, if the application requires it. This feature can be used, for instance, to adjust focusing strengths for each bunch or, within limits, for each subset of particles within a bunch.

The principle of the electron lens is based on the fact that the electron beam is magnetized. This means that the electron Larmor radius $r_L = p_\perp/(q_e B)$ is small compared to the transverse beam size r_b and it is also smaller or of the order of the typical distance between electrons $r_a = \sqrt[3]{3/(4\pi n_e)}$, to suppress intrabeam scattering. Here $p_\perp$ is the component of the electron momentum perpendicular to the magnetic field; its distribution depends on the cathode temperature, emission geometry, and field curvature. The quantity $n_e = j/(q_e v_\parallel)$ represents the electron density. In a perfectly magnetized beam, the electrons spiral around the field lines. Because current is conserved, the beam sizes r_g and r_m and current densities j_g and j_m at the gun and main solenoids, respectively, are related through the ratio of magnetic fields B_g and B_m:

$$B_g r_g^2 = B_m r_m^2, \quad \frac{j_g}{B_g} = \frac{j_m}{B_m}. \tag{1.3}$$

In other words, the ratio of the fields is used to control the compression or expansion of the beam.

2 Research areas based on the IOTA electron lens

2.1 Nonlinear Integrable Optics

A breakthrough in the study of dynamical systems was the realization that nonlinear integrable optics (NIO) can be implemented in an accelerator with certain lattice symmetries using special magnets or electron lenses [2–5, 33–36]. The design and first experimental results using nonlinear magnets in IOTA are described in refs. [6, 8–10]. In the case of electron lenses, two systems have been identified: (i) the McMillan electron lens and (ii) the axially symmetric thick lens.

2.1.1 McMillan lens

In refs. [37, 38], McMillan considered the stability of dynamical systems in general and described how to build one-dimensional symplectic nonlinear transformations with a conserved quantity, using geometrical and algebraic arguments. In particular, he showed that if the variables q and p (representing generic coordinates and momenta, for example) are transformed according to the nonlinear discrete map

$$\begin{cases} q_{n+1} = p_n \\ p_{n+1} = -q_n + \dfrac{2\epsilon p_n}{1+p_n^2} \end{cases}, \tag{2.1}$$

the quantity $I_{1D} = q^2p^2 + q^2 + p^2 - 2\epsilon qp$ is invariant. The value of ϵ parameterizes the strength of the nonlinearity.

The McMillan transformation can be generalized to two dimensions and applied to the transverse motion of a particle in a storage ring [2–4, 33]. The ring is modeled as two main elements: (i) a linear arc with equal amplitude functions $\beta_x = \beta_y = \hat{\beta}$ at the electron lens and equal phase advances $\mu_x = \mu_y = 2\pi\nu$ equal to an odd multiple of $\pi/2$, corresponding to a tune $\nu = 1/4$; (ii) a radial nonlinear kick $k_e r/\left[1 + (r/a)^2\right]$ at the electron lens, where k_e is the strength (eq. (1.1)) and a represents the

2021 JINST 16 P05002

width of the nonlinear distribution. In Cartesian coordinates $(x, x' = P_x/P_z, y, y' = P_y/P_z)$, where (x, y) is the transverse position and P is the particle momentum (with $P_x \ll P_z$ and $P_y \ll P_z$), the full one-turn symplectic map has the following form:

$$\begin{cases} x_{n+1} = \hat{\beta} x'_n \\ x'_{n+1} = -\dfrac{x_n}{\hat{\beta}} + \dfrac{\hat{\beta} k_e x'_n}{1 + \hat{\beta}^2 \frac{x'^2_n + y'^2_n}{a^2}} \\ y_{n+1} = \hat{\beta} y'_n \\ y'_{n+1} = -\dfrac{y_n}{\hat{\beta}} + \dfrac{\hat{\beta} k_e y'_n}{1 + \hat{\beta}^2 \frac{x'^2_n + y'^2_n}{a^2}} \end{cases} . \tag{2.2}$$

This map is integrable, having two independent invariants: the longitudinal component of the angular momentum

$$L_z = P_z \cdot (xy' - yx') \tag{2.3}$$

and the 2D McMillan invariant

$$I = \frac{1}{a^4}\left[\hat{\beta}^2\left(x^2x'^2 + y^2y'^2\right) + 2\hat{\beta}^2 xx'yy' + a^2\left(x^2 + y^2\right) + a^2\hat{\beta}^2\left(x'^2 + y'^2\right) - k_e a^2\hat{\beta}^2\left(xx' + yy'\right)\right]. \tag{2.4}$$

The required shape of the nonlinear kicks is generated by the following current-density distribution in the electron lens:

$$j(r) = \frac{j_0}{\left[1 + \left(\frac{r}{a}\right)^2\right]^2}. \tag{2.5}$$

The width is parameterized by the value of a, which is also the effective radius for the calculation of the total current: $I_e = j_0 \cdot (\pi a^2)$, as can be shown by integration.

In the linear limit (flat current-density distribution, or $r \ll a$), long-term stability of the iterated map requires $\left|\hat{\beta} k_e\right| < 2$. The tune of particles on axis is then

$$\nu = \frac{1}{2\pi} \arccos\left(\frac{\hat{\beta} k_e}{2}\right) \quad \text{(on axis)} \tag{2.6}$$

and it represents the maximum deviation from the unperturbed tune $\nu = 1/4$.

Because of the symmetry of the system, it is convenient to use radial and azimuthal coordinates and momenta

$$\begin{aligned} r &= \sqrt{x^2 + y^2}, & p_r &= \frac{xx' + yy'}{\sqrt{x^2 + y^2}}, \\ \theta &= \arctan2\,(y, x), & p_\theta &= \frac{xy' - yx'}{\sqrt{x^2 + y^2}}, \end{aligned} \tag{2.7}$$

and the conserved component of the angular momentum (divided by the constant longitudinal momentum):

$$L = L_z/P_z = r p_\theta. \tag{2.8}$$

In polar coordinates, the McMillan invariant is

$$I = \frac{\hat{\beta}^2}{a^2}\left(\frac{r^2 p_r^2}{a^2} + \frac{r^2}{\hat{\beta}^2} + p_r^2 + p_\theta^2 - k_e r p_r\right). \tag{2.9}$$

2021 JINST 16 P05002

The McMillan system can be further generalized to take into account the coupling effect of the electron-lens solenoid.

One of the main figures of merit of nonlinear integrable systems in accelerators is the achievable range of betatron tunes or tune spread, on which the stabilization mechanism (Landau damping) is based. In the electron-lens case, small amplitude particles experience the full intensity of the nonlinear kick, whereas particles at large amplitudes are almost unperturbed. For this nonlinear system, it is possible to obtain analytical expressions for the tunes as a function of dimensionless invariants [36]. In ref. [39], the detuning is expressed in terms of the physical parameters $\hat{\beta}$, k_e and a, with additional considerations for experiments in IOTA. For a 'weak' nonlinear McMillan lens ($\left|\hat{\beta}k_e\right| < 2$), eq. (2.6) yields the maximum detuning. In a strong nonlinear lens ($\left|\hat{\beta}k_e\right| \geq 2$), a subset of particles in the beam core experiences the full detuning $\Delta\nu = 0.25$. Therefore, the use of McMillan lenses for nonlinear integrable optics favors lattices with large $\hat{\beta}$ and k_e.

2.1.2 Axially symmetric thick lens

Another two-dimensional system that can be implemented with electron lenses is one where the axial component of a particle's angular momentum is conserved together with its Hamiltonian [2]. In this case, the nonlinear radial kick can have an arbitrary form. The main requirements are that (i) the kick is given in a region with equal beta functions and (ii) the rest of the ring can be modeled by round linear transformations with phase advances that are integer multiples of π. In a solenoid of length L and axial field B_z, the amplitude function can be kept constant at $\hat{\beta} = 2(B\rho)/B_z$, resulting in a phase advance $\Delta\mu = B_z L/[2(B\rho)] = L/\hat{\beta}$. In this case, the detuning is maximized by increasing the field and length of the solenoid. The effect of the electron lens can be modeled in a symplectic way by interleaving solenoid slices with thin nonlinear kicks.

2.2 Electron cooling

One of the key aspects of the IOTA research program is the understanding and control of space-charge-dominated beams. In general, these studies require a range of beam lifetimes and brightnesses and an electron cooler is extremely helpful in providing this flexibility. Moreover, the combination of electron cooling and nonlinear integrable lattices opens up the possibility of exceeding current proton beam brightness limits. Finally, an electron cooler will provide a flow of neutral hydrogen atoms through recombination that can be used for beam diagnostics [40].

2.2.1 Electron lens as electron cooler

The beam of the IOTA electron lens can be used for cooling protons if their average velocities match ($\beta_e = \beta_b$), corresponding to an electron kinetic energy of 1.36 keV for 2.5 MeV protons.

A set of parameters for proton cooling is shown in table 3. The injector can provide a maximum proton current of 8 mA and geometrical rms emittances of about 4 μm. The parameters are chosen to balance the dominant heating and cooling mechanisms, while achieving significant space-charge tune shifts. At injection, the beam practically fills the transverse and longitudinal apertures. The rms beam sizes correspond to about a quarter of the aperture limits.

The main processes leading to emittance growth are intrabeam scattering (IBS) and multiple Coulomb scattering (MCS) on the residual gas. For the parameters in table 3, transverse and

2021 JINST 16 P05002

longitudinal IBS emittance growth rates are of the order of 10 s. Rates are much faster for particles at small amplitudes. Adjustments of the cooler settings enable one to control the dependence of the cooling force on particle amplitude, thus providing a powerful mechanism for manipulating equilibrium beam distributions. IBS also introduces temperature exchanges between degrees of freedom, with time scales of about 3 s. Multiple Coulomb scattering gives emittance growth rates of 20–30 s.

Proton losses are caused by single Coulomb scattering (SCS) on the residual gas and by emittance growth. (Charge neutralization is discussed below.) In IOTA Run 2, with electrons, the equivalent atomic hydrogen pressure was 5×10^{-8} hPa. At these levels, the SCS maximum lifetime would be 17 minutes for a zero-emittance beam and considerably shorter for emittances comparable with the machine acceptance. With protons, vacuum levels need to be in the 10^{-9} hPa range or better, as electron cooling can counter emittance growth, but it cannot mitigate SCS losses.

The maximum electron beam current in the cooler is constrained by the space-charge voltage depression $\Delta V \simeq (30\,\mathrm{V/A})I_e/\beta_e$, which causes a corresponding spread in electron velocities. For cooling, this spread should be of the order of or smaller than the momentum spread of the protons. For this reason we set $I_e = 10$ mA. The lattice functions are $\beta_x = \beta_y = \hat{\beta} = 4$ m to minimize proton divergence. The electron beam radius $r_m = 12$ mm is chosen to cover at least 3 standard deviations of the proton beam size. Under these conditions, cooling times are of the order of 0.1 s and they are short compared to the IBS and MCS emittance growth rates, as required. The achievable cooling rates and equilibrium emittances depend on the features of the apparatus, such as the straightness

Table 3. Proton cooling scenario in IOTA.

Proton kinetic energy, K_b	2.5 MeV
Proton velocity parameter, β_b	0.073
Lattice functions at cooler, $\hat{\beta}$	4 m
Transverse machine acceptance, $A_{x,y}$	70 µm
Rf voltage, V_{rf}	0.81 kV
Rf harmonic number, h	4
Relative momentum acceptance, $\hat{\delta}_p$	5.3×10^{-3}
Number of protons per bunch, N_b	3.7×10^9
Proton beam current, I_b	1.3 mA
Transverse emittances (geom., rms), $\epsilon_{x,y}$	4.3 µm, 3.0 µm
Relative momentum spread, δ_p	1.3×10^{-3}
Bunch length, σ_s	0.8 m
Rms beam size at electron lens, $\sigma_{x,y}$	4.1 mm, 3.5 mm
Space-charge tune shift, $\Delta\nu_{\mathrm{sc}}$	−0.5
Electron kinetic energy, K_e	1.36 keV
Electron velocity parameter, β_e	0.073
Electron beam current, I_e	10 mA
Electron current-density distribution	Flat or semi-hollow
Electron beam radius, r_m	12 mm
Electron density, n_e	5.9×10^{12} m^{-3}

2021 JINST 16 P05002

of the solenoid field lines, the stability of the high-voltage power supplies, and vacuum. Reductions of the transverse emittances and momentum spread by about a factor 10 are achievable, with a corresponding increase in brightness.

2.2.2 Recombination rates

Radiative recombination $p + e^- \rightarrow H^0 + h\nu$ has proven to be a useful diagnostics for optimizing cooler settings and to determine the profile of the circulating beam. An overview is given in ref. [41], whereas ref. [42] describes a recent application. Neutral hydrogen is formed in a distribution of excited Rydberg states, which have to survive Lorentz stripping through the electron lens toroid and through the next ring dipole to be detected. For IOTA parameters and magnetic fields, atomic states up to quantum numbers $n = 12$ can survive. The corresponding recombination coefficient is $\alpha_r = 9.6 \times 10^{-19}\,\mathrm{m}^3/\mathrm{s}$ for a typical electron temperature $k_B T_e = 0.1\,\mathrm{eV}$. The coefficient is proportional to $1/\sqrt{k_B T_e}$. In the beam frame, transverse electron velocities significantly exceed those of protons, therefore the recombination rate has a weak dependence on proton velocity. The total recombination rate R is proportional to the fraction of the ring occupied by the cooler, L/C, and to the electron density n_e: $R = N_p \alpha_r n_e (L/C)/\gamma^2$. For the parameters in table 3, one obtains a rate $R = 1.5\,\mathrm{kHz}$, which is small enough not to significantly affect beam lifetime, but large enough for cooler tuning and for relatively fast profile measurements (see also section 4.4). As the beam cools, the size of the electron beam can be reduced, with a corresponding increase in electron density and recombination rate.

2.3 Tune-spread generation for Landau damping

Suppression of collective instabilities is typically achieved by a combination of feedback systems and Landau damping [43–45]. For multi-bunch beams, such feedback systems usually suppress the most unstable coupled-bunch and beam-beam modes. However, having limited bandwidths, these transverse dampers are normally inefficient for intra-bunch modes, and Landau damping is needed for their suppression. To make it possible, the spectrum of incoherent (individual particle) frequencies must overlap with the spectrum of the unstable collective modes, thus enabling the absorption of the collective energy by the resonant particles. The required frequency spread can be generated by (i) nonlinear focusing forces, such as those due to the charge distribution of the opposing beam in colliders, or (ii) by nonlinear magnets, usually octupoles. The first option is not available for machines with single beams, of course. Even in colliders, the effect is not present at injection or until the beams are brought into collisions, which themselves generate the required tune spread through the beam-beam head-on interaction. In octupoles, the transverse magnetic field near the beam axis is $B_y + iB_x = K_3 \cdot (x + iy)^3$, where K_3 is the strength of the element. The octupolar field distribution generates betatron frequency shifts proportional to the square of each particle's oscillation amplitude. As the energy E of the beam increases, the octupoles become less and less effective: the corresponding frequency spread scales as $1/E^2$, due to both the increased magnetic rigidity and the smaller beam size, whereas instability growth rates scale only as $1/E$, as the effect of the transverse beam size is negligible. As a consequence, one needs to increase the strength of these octupole magnets accordingly. For example, in the Tevatron proton-antiproton collider, with $E = 1\,\mathrm{TeV}$, there were 35 superconducting octupole magnets installed in 1-m-long cryostats and operated at currents up to 50 A. In the LHC at 6.5 TeV, 336 superconducting octupole magnets, each

2021 JINST 16 P05002

about 0.32 m long, operate at the maximum current of 550 A, and even that is not always sufficient to maintain beam stability above certain proton bunch intensities. The anticipated 50 TeV beam energy in the proton-proton Future Circular Collider (FCC-pp) [46, 47] would require a further increase in integrated octupole strength by a factor of more than 60 [48], which makes stabilization with octupoles extremely impractical. Another serious concern is that octupoles, operating at high strengths, induce significant nonlinear fields and frequency shifts for large-amplitude particles, with dangerous destabilizing effects that lead to increased particle losses and radiation loads [49].

Electron lenses are ideal for transverse Landau damping, as discussed in ref. [50]. The forces created by a single electron lens can easily introduce the required transverse nonlinear focusing. Unlike a nonlinear magnet, the electron lens generates the tune spread mainly at the beam core, thus mitigating dynamic aperture restrictions and lifetime degradation. (However, see also ref. [51] on the interplay between the number of electron lenses, lattice resonances, and dynamic aperture.)

An electron lens in IOTA provides a unique environment to study these effects experimentally. A controlled source of external wake fields ('antidamper' or 'waker') [52] will be used to induce coherent beam instabilities. A Gaussian electron lens will generate tunable amplitude-dependent frequency spreads. The instability thresholds and growth rates will be measured as a function of electron-lens beam size and current. For instance, calculations showed that the lens is most effective when its transverse rms size does not exceed that of the circulating beam. The possibility to vary the axial magnetic field and the beam emittances is also desirable. Advanced studies of Landau damping with space charge are discussed in section 2.5.

2.4 Space-charge compensation

Novel experimental studies of direct space-charge compensation (SCC) are one of the main research goals of IOTA. Space-charge neutralization and compensation are routinely used in one-pass systems, such as beam lines for low-energy beam transport (LEBT) and rf photoinjectors. In rings, SCC with electrons offers several advantages [32] and could enable higher intensities and brightnesses by reducing losses and emittance growth [51, 53–60]. Proof-of-principle experiments are needed to understand the limits of the method and to explore the stability of the system. For instance, it is not obvious how to mitigate the global effect of charge repulsion with a finite number of localized corrections (such as plasma lenses, beam-beam elements, residual-gas pressure bumps, etc.) over a fraction of the ring circumference. Challenges include the need for high compensating charge densities, the effects of beam-gas interactions, the generation of unwanted lattice distortions, and beam-plasma instabilities.

Two concepts of space-charge compensation related to electron lenses were developed:

electron column (*e-column*): The circulating beam ionizes the residual gas and secondary electrons are trapped in a Penning-Malmberg configuration [61, 62] that mirrors as closely as possible the charge density of the beam [63, 64]. No electron gun or collector are used in this case.

space-charge-compensating electron lens (*SCC e-lens*): The electron gun generates an electron beam with the required intensity and current-density profile, transversely and possibly also in time.

2021 JINST 16 P05002

2.4.1 Electron column

Early experiments at the Budker Institute for Nuclear Physics in Novosibirsk showed that space-charge limits in a ring could be exceeded by using trapped compensating plasmas [65–69]. Later, the tune shifts induced by trapped electrons could be measured in tests at the Tevatron [70]. However, experiments were limited by vacuum pressures, beam instabilities, poor control of the plasma, or lack of diagnostics. The benefits of using electron columns in the Fermilab Booster were calculated and discussed in refs. [55, 56]. An interesting set of experiments on the interaction of a proton beam with a trapped electron plasma column were conducted at the Indiana University Cyclotron Facility (IUCF) [71, 72].

The goals of experiments in IOTA are to characterize the evolution of the non-neutral plasma and to measure the effects on the circulating beam.

The electron column is fed by the residual-gas ionization caused by the circulating beam. Cross sections for these processes are collected in ref. [73]. They have typical values of $\sigma_i = 1.7{\times}10^{-21}$ m^2 for protons at 2.5 MeV.

The loading time of the column is determined by ionization rate and by the confining forces. The value of the solenoid field B_m should be strong enough to trap electrons radially, while letting ions escape. Longitudinally, electrons are confined with negatively biased electrodes at voltage V_e. This bias voltage also drains ions. Ion recombination and other collisional processes influence the evolution of the electron column as well.

Considerable progress has been made in modeling electron columns in IOTA [74–78]. Numerical simulations are challenging because of the very different time scales involved: cyclotron motion, plasma oscillations, and beam revolution period. Also, a large number of particles is necessary to track density fluctuations and halo effects. Assuming a coasting proton beam, the optimization of the confining fields and residual gas pressures using the WARP particle-in-cell code [79, 80] was discussed in ref. [75]. Typical values for IOTA are $B_m = 0.1$ T and $V_e = -5$ V. Local residual gas pressures of $p = 5 \times 10^{-4}$ hPa are necessary to get a neutralization time $\tau_N \sim 1\,\mu$s, comparable to the proton revolution time $\tau_{\rm rev} = 1.8\,\mu$s. However, at these pressures, proton lifetime due to single Coulomb scattering and emittance growth is of the order of 0.1 s. This regime may be useful for experimental demonstrations; on the other hand, lower pressures may be sufficient to mitigate slower instabilities. The time structure of the proton beam and the evolution of the column between two beam traversals was studied in refs. [76, 77]. The first model including the full ring with space charge in Synergia [81, 82] was presented in ref. [78]. The next challenge in numerical simulations will be the integration of plasma evolution and ring space charge. Further information on the current status of electron column studies can be found in ref. [83].

IOTA provides unique research opportunities for novel studies and systematic measurements of electron columns. One of the most challenging aspects is to accommodate a gas injection system to vary the local residual gas pressure over a wide range, while preserving vacuum levels in the rest of the ring.

2.4.2 Space-charge-compensating electron lens

Strong space-charge forces in high-brightness proton beams drive particles to lattice resonances, causing emittance growth, losses and lifetime degradation. Typically, such effects become intoler-

2021 JINST 16 P05002

able when the space-charge tune-shift parameter $\Delta\nu_{sc}$ reaches the range -0.25 to -0.50. To reduce these detrimental effects, it was suggested to use electron lenses to compensate the space-charge forces [53]. Further analysis and computer modeling [51, 54, 58–60] indicated that compensation with electron lenses may enable an accelerator to exceed the space-charge limit and to operate with much larger tune-shift parameters, up to -1.0. The SCC e-lens should have a transverse current-density profile close to that of the proton beam. Interaction of protons with one or more of such devices per turn will result in a reduction of the spread in tunes from $\Delta\nu_{sc}$ to $\Delta\nu_{sc} \cdot (1-\eta)$, where η is the degree of compensation (in the non-relativistic case). The resulting proton footprint becomes small enough to avoid crossing strong lattice resonances, reducing emittance growth and losses.

Experimental SCC studies in IOTA are needed to explore many effects arising in real accelerators and electron lenses. Both bunched and coasting beams can be used to extend the range of parameters. For instance, the optimal degree of compensation η, predicted to be less than 1, needs to be determined experimentally. Studies showed that the longitudinal profile of the electron current pulse is also critical [51, 57, 59, 60]. One of the challenges lies in the generation of fast electron pulses that match the short bunches in a storage ring. The current state of the art is sufficient for the first phase of compensation experiments in IOTA. The full definition of pulse timing requirements for the SCC e-lens is underway. We note that a similar research program, targeted to the synchrotrons for FAIR, is being carried out at GSI [31, 58, 84].

2.5 Other advanced studies of beam dynamics and stability

As a research machine, IOTA is designed to provide a flexible environment for novel investigations under unique experimental conditions. Several advanced research topics related to electron lenses are at the conceptual stage. Here we summarize some of them.

The interplay between destabilizing mechanisms, such as space charge and impedances, and mitigation strategies, like cooling, Landau damping, and feedback are of particular scientific interest and technological relevance. For instance, we plan to study the transverse coherent stability limits for bunched beams with strong space charge, beam cooling and nonlinear focusing elements, such as the electron lens. Because machine impedances in IOTA are negligible for proton dynamics, a tunable digital transverse feedback system will be installed to emulate the effects of wakefields [52] (as mentioned in section 2.3).

The behavior of coherent instabilities in the presence of strong space-charge forces is of great interest. Studies presented in refs. [85, 86] predicted that there are regimes for which Landau damping with electron lenses, described in section 2.3, is effective under space-charge conditions as well. Experiments with protons in IOTA could shed light on this topic, with a significant impact on the performance of high-intensity accelerators. The IOTA electron lens can also be used for further studies of the head-tail instability due to the skew wake of the magnetized electron beam, predicted in ref. [87].

In addition to providing a range of beam parameters for various experiments, the presence of an electron cooler in IOTA enables the investigation of several scientific questions. For instance, when electron cooling is limited by instabilities or by space-charge tune spread, does nonlinear integrable optics combined with cooling enable higher brightnesses? Is it possible to attain record-high stable space-charge tune shifts in the presence of beam cooling by varying the electron beam density distribution and transverse focusing in the rest of the machine? The basic scenario includes an

2021 JINST 16 P05002

electron lens configured for cooling, as described in section 2.2. Integrability and tune spreads are provided separately by nonlinear magnets. An appealing but more challenging solution would be to combine in the same device (the electron lens) both cooling and nonlinear focusing, although preliminary studies indicate that it is difficult to combine both the constraints of cooling and the high currents needed to achieve sizable tune spreads. A related topic, the use of a McMillan electron lens to mitigate space charge, is discussed in refs. [88, 89]

3 Design and specifications

The research program based on the IOTA electron lens is wide and exciting. The main challenge is to incorporate several functions in a single compact device. Beam physics goals and operational considerations dictate the functional requirements. A summary of the main parameters is presented in table 2. Here we discuss some of the design considerations.

3.1 General layout

The electron-lens assembly must fit in one of the IOTA straight sections (DR in figure 1). The maximum available axial length is 1.4 m. Displacing the quadrupoles on each end to increase this length would affect the symmetry of the ring and the minimum achievable amplitude function $\hat{\beta}$. Taking into account the space needed for the toroidal section and dipole correctors, this leaves about 0.7 m for the main solenoid.

The low-energy electron beam co-propagates with the circulating beam to make electron cooling possible. This choice has a small effect on the maximum achievable kicks (eq. (1.1)).

3.2 Storage-ring lattice

For nonlinear integrable optics, the ring lattice must provide the required phase advances and amplitude functions. The ring was designed to control phase advances at the level of 10^{-3} and beta functions within 1%. Experiments on single-particle dynamics will be conducted with a pencil beam of electrons, observing tunes and intensities as a function of kicker amplitude with turn-by-turn (TBT) beam position monitors (BPMs). For the McMillan lens, the amplitude function $\hat{\beta}$ should be as large as possible, whereas the axially symmetric thick-lens configuration requires a large solenoidal field and, therefore, a small beta function. The IOTA focusing lattice was designed to provide equal amplitude functions around the region of the electron lens in the range $2\,\mathrm{m} \leq \hat{\beta} \leq 4\,\mathrm{m}$ and with vanishing slope (Courant-Snyder parameters $\alpha_{x,y} = 0$). The corresponding values of the main solenoid field $B_m = 2(B\rho)/\hat{\beta}$ are reported in table 4. For lattice and momentum flexibility, we require that the main solenoid provide at least $B_m = 0.7\,\mathrm{T}$ in operations, with a maximum of 0.8 T for the engineering design as a safety margin [90]. For electron cooling, it is preferable to use the larger beta function values and minimize beam divergence. This range of beta functions is also appropriate for space-charge compensation, where electron lens and circulating proton beam sizes should be matched.

The IOTA lattices for NIO experiments are shown in figure 3. The coupled lattice functions $\beta_x \equiv \beta_1$ (black) and $\beta_y \equiv \beta_2$ (red, both on the left vertical scale) (Edwards-Teng parameterization [91–93], calculated with MAD-X [94]) and the horizontal dispersion D_x (green, on the right vertical scale) are plotted as a function of the distance s along the ring, starting from the injection

2021 JINST 16 P05002

point (see also figure 1). The location of the electron lens is highlighted in orange. The left plot refers to the McMillan lens case, with $\hat{\beta} = 4$ m, whereas the right plot is for the axially symmetric thick lens, where $\hat{\beta} = 2$ m.

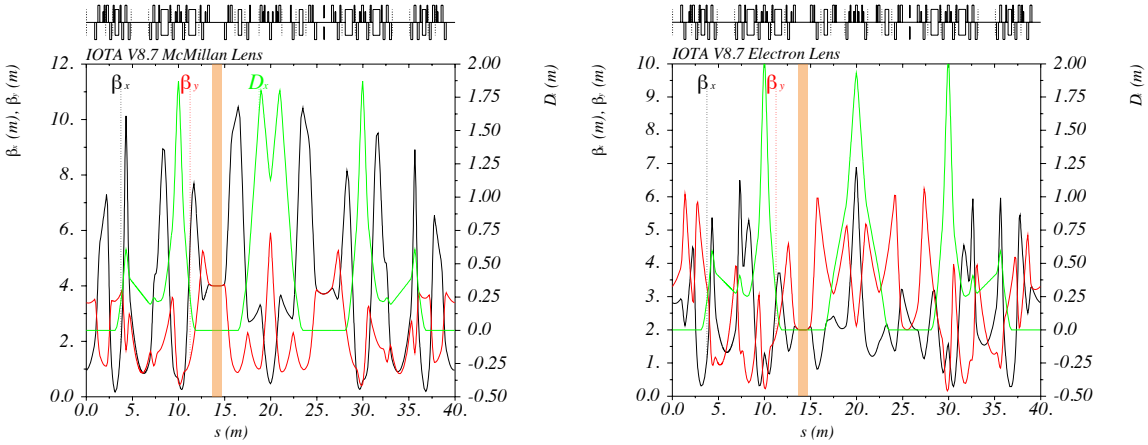

Figure 3. IOTA lattices for electron lens experiments.

3.3 Magnetic system

The magnetic system has several functions. First of all, it should transport the beam from the electron gun to the overlap region and, finally, to the collector with an efficiency > 99% for beam radii < 15 mm and for all magnetic field configurations. The electron beam should be magnetized, i.e. with a Larmor radius much smaller than the typical beam sizes and smaller than the average separation between individual electrons, as discussed in section 1. Secondly, the ratio of the gun and main solenoid fields B_g/B_m determines the compression and therefore the beam size and affects the temperature of the beam in the overlap region. Moreover, the field stabilizes e-p beam oscillations [87, 95, 96].

The bore of the main solenoid must be large enough to accommodate the beam pipe, flanges, and feedthroughs for instrumentation. In the current design, the bore diameter is 115 mm. The main solenoid should be as long as possible, with a minimum length of 0.7 m. The minimum magnetic field seen by the low-energy electron beam should be as large as possible and at least 0.1 T. The distance between the axis of the main solenoid and the trajectory of the low-energy beam with correctors off should be within 1 mm. For alignment with the circulating beam, the trajectory of the low-energy beam in the main solenoid should be adjustable in both horizontal and vertical positions and angles. The position adjustments should have a range of ±10 mm with 0.03 mm resolution.

Table 4. Lattice requirements on main solenoid field.

Species	Kinetic Energy [MeV]	Magnetic Rigidity [T m]	Main Solenoid Field [T] $\hat{\beta} = 2$ m	Main Solenoid Field [T] $\hat{\beta} = 4$ m
Electrons	150	0.50	0.50	0.25
Protons	2.5	0.23	0.23	0.11

2021 JINST 16 P05002

Angles should be adjustable in the range ±5 mrad with resolution 50 µrad. Field distortions in the good field region of the main solenoid should be $(B_\perp/B_z) < 2 \times 10^{-4}$. This requirement is mainly dictated by electron cooling. The good field region of the main solenoid should be at least 0.6 m long and have a transverse diameter of at least 30 mm, corresponding to more than half of the IOTA aperture.

3.4 High-voltage system

We plan to use electron beams up to 10 keV. Several electron guns we designed and built have been operated at these voltages without breakdowns. Moreover, at these energies, emission of X-rays is negligible.

For beam extraction, in addition to using the electron gun in direct-current (DC) mode, we plan to pulse the cathode-anode voltage with a high-voltage modulator. State-of-art devices with rise times (10%–90%) of less than 100 ns, repetition rates up to 50 kHz, and pulse widths as short as 200 ns are adequate for most applications identified so far. Electron guns have anode-cathode capacitances of the order of 50 pF, which, together with the associated electronics, limit the rise time and repetition rate of the electron pulses. Gating electron-gun emission with grids is possible, but it may cause losses and profile distortions. Matching the longitudinal distribution of the circulating bunches (a few nanoseconds for electrons and a few tens of nanoseconds for protons) requires further developments in electron-gun and modulator technology.

The high-voltage circuit includes separate bias voltages for the cathode, the electrodes and the collector. With this arrangement, the beam is decelerated before depositing its energy on the collector. In addition, the functions of high-current supply and precision beam energy setting are separated.

3.5 Electron beam

The properties of the electron beam are of course key in an electron lens. For nonlinear integrable optics, the current-density distribution should be sufficient to generate large tune spreads within the machine aperture. To exploit the full detuning $\Delta\nu = 0.25$ in the McMillan case, we need $|k_e| \geq 2/\hat{\beta}$. A high current requirement comes from a scenario with 150 MeV circulating electrons, $\hat{\beta} = 4$ m and $k_e = 0.5\,\mathrm{m}^{-1}$, resulting in $j_m \geq 10\,\mathrm{A/cm}^2$ for a typical electron-lens energy of 6 keV. The size of the low-energy beam should be larger than the size of the pencil beam and at the same time small enough so that the full detuning can be achieved within the available good-field aperture of the machine (about 12 mm in radius). For the McMillan lens, we choose the parameter a (eq. (2.5)) in the main solenoid $a_m = 2$ mm. The required beam current is therefore $I_e = j_m \cdot (\pi a_m^2) = 1.3$ A at 6 kV, which can be achieved in an electron gun with perveance $P = 2.8\,\mu\mathrm{A/V}^{3/2}$. Other scenarios and applications require less current.

The ability of generating and transporting different transverse current-density profiles is one of the strengths of electron lenses. This is usually done by replacing the electron gun, although some limited flexibility can be achieved by controlling electrode potentials within the same source. For nonlinear integrable optics, we require a McMillan profile (eq. (2.5)), which is a new development. Tolerance studies on the required accuracy are underway. McMillan or Gaussian profiles are adequate for NIO experiments with axially symmetric thick lenses. For electron cooling, a flat or

2021 JINST 16 P05002

partially hollow profile is used. For the SCC e-lens and for tune-spread generation, a Gaussian distribution can be employed in the first round of experiments.

Preservation of the profile from the source to the overlap region relies on the strength and quality of the magnetic fields. Distortions of the beam trajectory and of the current-density profile arise mainly from field curvature (in the toroidal section, for instance) and from self fields. They must be evaluated and mitigated, usually by reducing imperfections and by increasing the minimum axial field seen by the beam. Because of the $B \times \nabla B$ force, the toroidal sections introduce a shift in the trajectory of the centers of gyration perpendicular to the plane of the lens, which must be kept within about 2 mm. As regards the current-density profiles, experimentally one observes that they scale with electron beam current and confining axial field according to the expected space-charge evolution [97, 98]. In particular, similar profiles are obtained for a given family of experimental conditions with constant ratio $\sqrt{V}/B$, where B represents the effective average value of the axial fields, assumed to scale proportionally ($B \propto B_m \propto B_g$). This ratio is related to the space-charge evolution number $g = \omega_D \cdot \tau_e \propto \sqrt{V}/B$, representing the number of $E \times B$ rotations in the propagation time τ_e, with $\omega_D \equiv \omega_{pe}^2/(2\omega_{ce})$ the diocotron (slipping-stream) angular frequency, $\omega_{pe} = \sqrt{q_e^2 n_e/(\epsilon_0 m_e)}$ the plasma angular frequency, and $\omega_{ce} = q_e B/(\gamma_\perp m_e)$ the cyclotron frequency of the magnetically confined electrons [99]. Beyond analytical estimates, numerical simulations are necessary to evaluate the effects of distortions on profiles. A study was described in ref. [100], using the BENDER particle-in-cell code [101]. Other efforts based on the WARP code [79, 80] and on the commercial software COMSOL [102] and CST STUDIO SUITE [103] are ongoing. In the end, the requirements on electron beam profiles translate into an interplay between source geometry, accelerating voltages, and magnetic field configurations.

3.6 Vacuum system

The vacuum system must maintain pressures below 10^{-6} hPa in the region of the heated cathode. The assembly is designed so that electron guns can be valved out, swapped and pumped down in a few hours. In the overlap region, residual-gas pressures seen by the circulating beam should be less than 10^{-9} hPa for electrons and 10^{-10} hPa for protons. Controlled gas injection for e-column applications and, possibly, for ionization profile monitors (section 4.4) presents a challenge and solutions are under study.

4 Experimental apparatus

The general layout of the IOTA electron lens is shown in figure 2. Here we discuss some of the features of the subsystems.

4.1 Magnetic system

The current configuration of the magnetic system includes the following components:

- 1 gun and 1 collector solenoid, with 4 corrector coils each.
- 2 transport solenoids, with 4 corrector coils each.
- 2 short solenoids in each of the 2 toroidal sections.

2021 JINST 16 P05002

- 1 main solenoid with 8 corrector coils: 4 short ones upstream for horizontal and vertical position adjustments and 4 long ones downstream for horizontal and vertical angle adjustments.
- 2 orbit correctors (not shown in figure 2) for the circulating beam to compensate for the transverse kicks due to the toroidal sections, 1 just upstream and 1 downstream of the electron lens.

The gun and collector solenoids are available. They were recovered from one of the Tevatron electron lenses (TEL-2) [20]. The transport solenoids, the toroidal sections and the orbit correctors need to be built. For the main solenoid, we are considering a conduction-cooled, cryogen-free superconducting solenoid. A view is shown in figure 4. This choice implies compact coils, improved field quality, and lower power consumption compared to a resistive solenoid. These systems are reliable and well supported and cool-down times are compatible with IOTA operations. The design of the coils and quench protection system is underway. The current status of the design is described in detail in refs. [90, 104].

4.2 Electron sources

Several electron guns were built at Fermilab over the course of the years for the Tevatron electron lenses, as prototypes for the LHC, and for general research and technological developments. They are based on thermionic emission from porous tungsten dispenser cathodes with BaO:CaO:Al_2O_3 impregnant, operating at temperatures around 1200 K. These designs are robust and reproducible and routinely yield current densities of the order of 4 A/cm^2. New technological developments have made designs based on scandate cathodes viable for aerospace applications and accelerators. In collaboration with CERN [26, 105], they are being considered in cases where larger current densities or lower operating temperatures are required. Although we have not been able to pursue it so far, another development that would significantly simplify the design of compact electron lenses are axially symmetric sources and collectors mounted around the main beam pipe, eliminating the need for the toroidal sections [106–108].

Figure 5 shows a photograph of the 10-mm-diameter electron gun used in the Tevatron for beam-beam compensation studies. Measurements of the current-density profile taken at the Fermilab

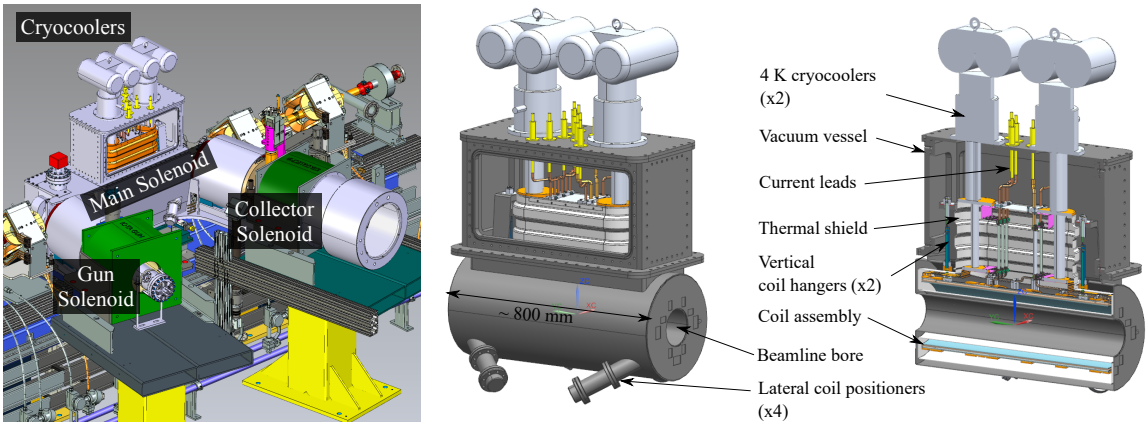

Figure 4. Layout of the superconducting option for the main solenoid.

2021 JINST 16 P05002

electron-lens test stand (see section 4.5) are also shown. This electron source can be reused in IOTA for NIO studies, in the SCC e-lens configuration, or for the generation of tune spreads. New cathodes are available if replacements are needed.

For the IOTA research program, it is important to maintain and develop the capability to design and build new electron sources, such as the McMillan electron gun for NIO or flat and semi-hollow guns for electron cooling.

4.3 Collector

The collector is reused from one of the Tevatron electron lenses (TEL-2) [20]. It is made of copper with a ceramic gap insulating it from the vacuum chamber. The assembly is water cooled and has a power rating of 50 kW, well exceeding the maximum beam power anticipated for the IOTA electron lens.

4.4 Instrumentation and diagnostics

Beam diagnostics is critical for a research machine like IOTA. Here we mention instrumentation that is directly related to the electron lens, as well as other diagnostic devices that are relevant for the research program.

The current and pulse structure of the low-energy electron beam is measured with 2 passive beam current transformers, one at the cathode and one at the collector.

A diagnostic station was designed to provide profile measurements of the magnetized beam (figure 6). The station is located just upstream of the collector, to minimize its influence on beam dynamics in the overlap region. If necessary, another station could be installed just downstream of the electron gun to measure beam properties at the source. At low electron beam currents ($\lesssim$ 100 mA peak), fast profile imaging is provided by a rectractable YAG screen and a CCD camera. At higher intensities, a TZM-alloy plate with a pinhole and Faraday cup can be scanned across the beam to measure current density as a function of transverse position. Most components have been procured. The stations need to be assembled and tested. A similar setup is used for the RHIC electron lenses, as described in refs. [109, 110].

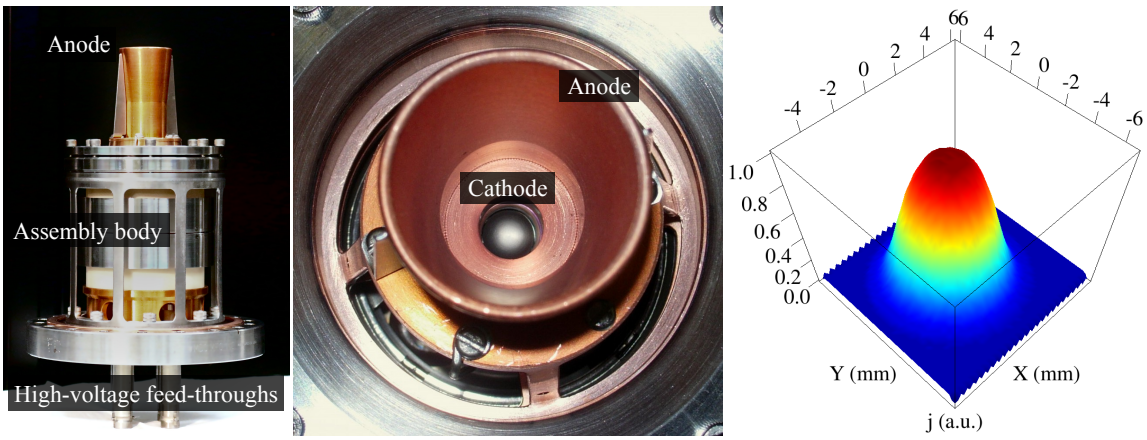

Figure 5. Gaussian electron gun.

2021 JINST 16 P05002

In addition to the 21 button BPMs in the ring, 2 BPMs are included in the beam pipe inside the main solenoid for aligning the low-energy electron beam with the circulating beam. The current design includes strip-line pickups to enhance the signal and to accommodate the different time structures of electron-lens pulses, 150 MeV electrons and 2.5 MeV circulating protons. However, preliminary estimates indicated that button BPMs may also be adequate.

A set of 5 biased diagonally-split cylindrical electrodes is foreseen for the central section of the electron lens to cover several functions. The electrodes can be used as transverse and longitudinal pickups for additional beam position monitoring, pulse timing and, in the case of the e-column, to detect plasma oscillations. When biased, they will be used for clearing trapped ions in the circulating electron beam or to confine the electron column during proton operations. The measured bias current is an indication of electron or ion fluxes. One of the electrodes, with 8 sectors, may be employed to implement the 'rotating-wall' technique to study the stabilization of the electron column [62, 111, 112].

Advanced instrumentation to measure beam intensities, emittances and losses over the time scales of instability growth is essential to characterize the dynamics of high-brightness space-charge-dominated proton beams. Various options are being considered for continuous monitoring of proton transverse profiles and emittances. The first option is a compact gas-sheet profile monitor (GSPM), which was built and characterized [9, 113]. In the GSPM, a compressed gas (N_2) is forced through a nozzle. As the gas travels downstream, it exhibits molecular flow due to the high Knudsen number. The gas then reaches a skimmer, which removes any molecules with significant divergence and provides the final shape. The resulting sheet is then injected at an angle transversely to the direction of the proton beam. The beam ionizes the gas and the ions are extracted by a series of annular electrodes. Microchannel plates (MCPs) convert the ions to electrons and yield a typical amplification factor of 10^3—10^6. The electrons impinge on a scintillator screen, and the image is recorded by a high-speed CCD camera for reconstruction of the transverse beam distribution.

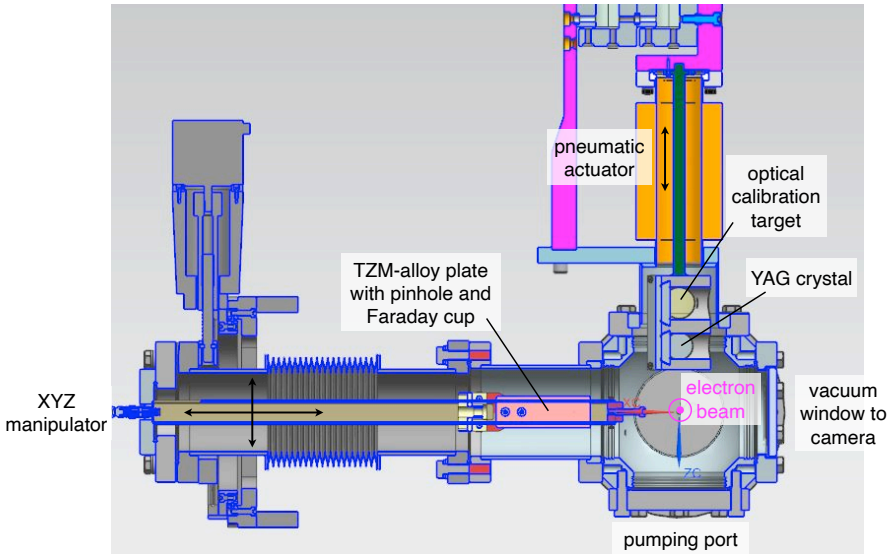

Figure 6. Layout of the diagnostic station.

2021 JINST 16 P05002

An option for fast, turn-by-turn beam size diagnostics is an ionization profile monitor (IPM). This device collects ions from ionizations induced by the proton beam to generate a beam profile. The amount of signal is proportional to the ionization cross section and the gas density. The gas source can either be the residual gas or an injected gas. Horizontal and vertical IPMs have been recently used for advanced studies in the Fermilab Booster proton synchrotron [114, 115]. In IOTA, the residual gas pressure will be lower than it is in the Booster. However, the ionization cross section for 2.5 MeV protons is two orders of magnitudes larger, yielding comparable signal rates. In IOTA, IPMs similar to those in the Booster, i.e. without external guiding magnetic field, will have another important advantage. According to an analysis presented in ref. [116], the expansion of the ions due to the charge of the proton beams is minimal (of the order of 1%, compared to factors as large as 2 in the Booster), introducing negligible systematics in the turn-by-turn reconstruction of the proton beam profiles.

Finally, operation of the IOTA electron lens as an electron cooler opens up an additional diagnostic opportunity — the detection of neutral hydrogen from recombination, as described in section 2.2. A recombination monitor will be installed behind the first dipole magnet downstream of the electron lens (M4R in figure 1) to detect neutral hydrogen atoms H^0 formed in the electron lens when the velocity of the magnetized beam matches that of the circulating protons. The rate of neutralization events is used to tune the cooler settings. In addition, the transverse distribution of H^0 provides a relatively fast ($\sim$ 1 s), minimally invasive estimate of the proton distribution. As a detector, we are considering microchannel plates and a phosphor screen read out with a CCD camera or a position-sensitive silicon detector.

The range of 2.5 MeV protons in metal is smaller than the beam pipe thickness. Proton losses can only be directly monitored inside the vacuum chamber. Prototype in-vacuum diamond detectors have been used in other machines [117, 118]. They are being considered for proton loss measurements in IOTA as well.

The inclusion of an additional instrument for the IOTA electron lens is under study. A pickup antenna could be installed in the vacuum chamber inside the main solenoid to sense cyclotron radiation emitted by the magnetized electrons. Such a receiver can be used to monitor the electron plasma density and temperature (besides providing a very accurate measurement of the magnetic field) by recording the position, intensity and width of the cyclotron frequency peak (expected at 2.8 GHz in a 0.1 T field, for instance). The device was proposed for electron cooling [119–121] and similar systems were applied to other precision measurements [122–124]. An operational system would provide a new sensitive tool for electron lenses, especially for electron cooling and electron columns.

4.5 The Fermilab electron-lens test stand

The Fermilab electron-lens test stand is a laboratory dedicated to the study of beam physics and technology related to electron lenses. It was set up in the late 1990s in support of the first electron lenses, built for the Tevatron collider [125, 126]. It has been used to characterize high-perveance electron guns, to measure the effects of space charge on magnetized beam dynamics, and to study trapped plasma columns. In recent years, it was instrumental in the development of hollow electron lenses for beam halo control in the Tevatron [22] and in the LHC [29]. The IOTA research program on nonlinear integrable optics relies on electron guns with specific current-density distributions. Electron sources for cooling and space-charge compensation can also be tested here.

2021 JINST 16 P05002

This test stand has been operational for over 20 years and it has been the only electron-lens test stand in the world for long periods of time. A similar facility was built at Brookhaven National Laboratory to support the RHIC electron-lens project [109], but it has since been decommissioned. A test stand for the HL-LHC hollow electron lenses is currently being developed at CERN.

The main experimental apparatus consists of a pulsed electron gun, a straight beam line with pickup electrodes, and a water-cooled collector (figure 7). The vacuum chamber is surrounded by three, independently powered resistive solenoids: the gun solenoid, the main solenoid, and the collector solenoid. The maximum magnetic field is 0.4 T. Magnetic correctors are used to steer the electron beam. End-plates in the metal shell of the solenoid are used to improve the uniformity of the axial magnetic field. The device is supported and aligned on a girder.

Current to the solenoids is provided by four 150 kW, 5 kA power converters. In steady state, at the maximum magnetic field, the solenoids dissipate about 210 kW through the low-conductivity water circuits. The vacuum system includes a diaphragm and turbomolecular pump for fore vacuum and ion-getter pumps to reach the operating pressures, which are typically 10^{-7} hPa to 10^{-8} hPa. The inner diameter of the beam pipe and of the pickup electrodes is 60 mm.

The cathode of the electron gun can be biased down to $V_c = -10\,\mathrm{kV}$. The anode is pulsed from V_c up to 0 V for beam extraction at a maximum rate of 10 kHz by a high-voltage modulator.

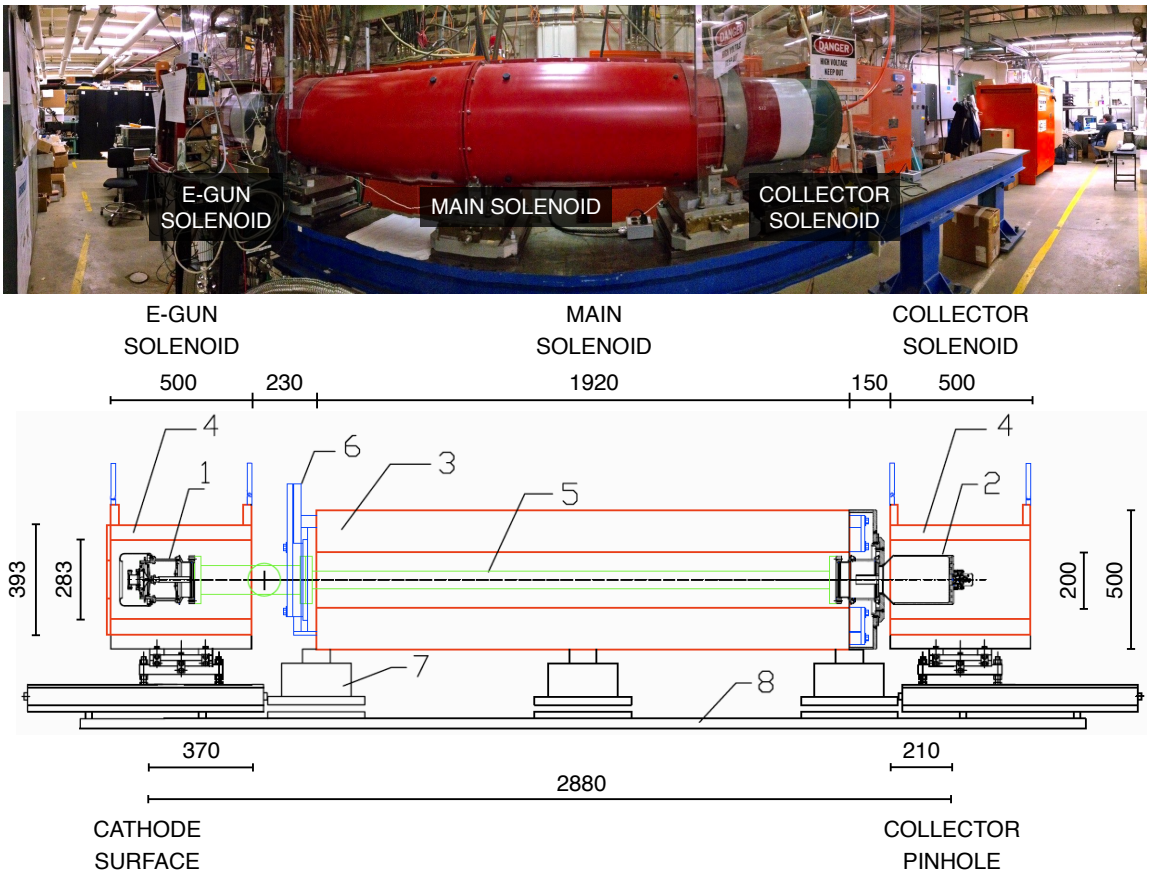

Figure 7. The Fermilab electron-lens test stand. Dimensions are in millimeters. (Photo: Valentina Previtali / Fermilab)

2021 JINST 16 P05002

Typical pulse widths are between 200 ns and 20 µs. The control system is integrated with the rest of the Fermilab complex (ACNET). However, solenoid settings, high-voltage power supplies and cathode filament heater are often controlled locally in manual mode.

Several types of electron guns have been designed and built to provide different intensities, beam sizes, and current-density profiles (flat, Gaussian, hollow, etc.). The electron source is typically based on a thermionic cathode. The electron-gun assemblies share the similar form factors and the same flange adapters, so that they can be swapped easily.

The total beam current and pulse shape are measured with passive transformers at the cathode and at the collector. The current-density profiles are measured by recording the average current through a 0.2-mm-diameter pinhole in the collector, as a function of the settings of the horizontal and vertical magnetic correctors. An example of current-density profile measurement is shown in figure 5 above.

5 Conclusions

An exciting beam physics program is being carried out with the IOTA storage ring at Fermilab and the first results have been published. The IOTA electron lens will be a key component of upcoming studies on nonlinear integrable optics, space-charge compensation, electron cooling, and the stability of intense beams in general. For the first time, several functions are being combined in a compact device, yielding technical challenges but also new opportunities for research, training, and collaboration.

Acknowledgments

We would like to thank the Beam Dynamics Panel of the International Committee for Future Accelerators (ICFA) and its chair, prof. I. Hofmann, for curating this Special Issue on electron lenses. Our Fermilab colleagues and the whole FAST/IOTA team made this research possible, in particular D. Broemmelsiek, D. Edstrom, D. Franck, W. Johnson (retired), V. Kashikhin, J. Leibfritz, M. McGee (retired), L. Nobrega, M. Obryki, J. Thangaraj, L. Valerio and T. Zolkin. We have greatly benefited from the growing international community of electron-lens experts, including W. Fischer and X. Gu of Brookhaven National Laboratory, A. Levichev and D. Nikiforov of the Budker Institute of Nuclear Physics, and D. Mirarchi, S. Redaelli, A. Rossi, and S. Sadovich of CERN. Prof. A. Pikkarainen of Kemi Unversity of Applied Sciences (Finland) and students H. Schmuul and J. Suopajärvi contributed to the mechanical designs. This work was supported in part by Phase I Small Business Innovation Research (SBIR) Award No. DE-SC0020928 of the U.S. Department of Energy. This manuscript has been authored by Fermi Research Alliance, LLC under Contract No. DE-AC02-07CH11359 with the U.S. Department of Energy, Office of Science, Office of High Energy Physics.

References

[1] S. Antipov et al., *IOTA (Integrable Optics Test Accelerator): Facility and Experimental Beam Physics Program*, 2017 *JINST* **12** T03002 [arXiv:1612.06289].

2021 JINST 16 P05002

[2] A.G. Ruggiero, *Integrability of the two-dimensional beam-beam interaction in a special case*, *Part. Accel.* **12** (1982) 45.

[3] V.V. Danilov and E.A. Perevedentsev, *On invariants and integrability in nonlinear accelerator optics*, Tech. Rep., SL-NOTE-94-74-AP, CERN, Geneva, Switzerland (1994).

[4] V.V. Danilov and E.A. Perevedentsev, *Two examples of integrable systems with round colliding beams*, in *Proceedings of the IEEE Particle Accelerator Conference*, Vancouver, BC, Canada, 16 May 1997, pp. 1759–1761.

[5] V. Danilov and S. Nagaitsev, *Nonlinear Accelerator Lattices with One and Two Analytic Invariants*, *Phys. Rev. ST Accel. Beams* **13** (2010) 084002 [arXiv:1003.0644].

[6] S.A. Antipov, S. Nagaitsev and A. Valishev, *Single-Particle Dynamics in a Nonlinear Accelerator Lattice: Attaining a Large Tune Spread with Octupoles in IOTA*, 2017 *JINST* **12** P04008 [arXiv:1604.08565].

[7] C.E. Mitchell, R.D. Ryne and K. Hwang, *Bifurcation analysis of nonlinear Hamiltonian dynamics in the Fermilab Integrable Optics Test Accelerator*, *Phys. Rev. Accel. Beams* **23** (2020) 064002.

[8] A. Valishev, N. Kuklev, A. Romanov, G. Stancari and S. Szustkowski, *Nonlinear integrable optics (NIO) in IOTA Run 2*, Tech. Rep., Beams-doc-8871, Fermilab (2020).

[9] S. Szustkowski, *Nonlinear Integrable Optics Beam Dynamics Experiment and Diagnostics*, Ph.D. thesis, Northern Illinois University, DeKalb, Illinois, U.S.A. (2020).

[10] N. Kuklev, *Nonlinear integrable optics studies at IOTA*, Tech. Rep., Beams-doc-8916, Fermilab (2020).

[11] M. Hofer, R. Tomás Garcia, A. Romanov, G. Stancari, A. Valishev, N. Kuklev et al., *Nonlinear optics measurements in IOTA*, Tech. Rep., FERMILAB-FN-1119-AD, CERN-ACC-NOTE-2021-0010, CERN (2021).

[12] I. Lobach, V. Lebedev, S. Nagaitsev, A. Romanov, G. Stancari, A. Valishev et al., *Statistical properties of spontaneous synchrotron radiation with arbitrary degree of coherence*, *Phys. Rev. Accel. Beams* **23** (2020) 090703 [arXiv:1912.06737].

[13] I. Lobach, S. Nagaitsev, V. Lebedev, A. Romanov, G. Stancari, A. Valishev et al., *Transverse beam emittance measurement by undulator radiation power noise*, *Phys. Rev. Lett.* **126** (2021) 134802 [arXiv:2012.00832].

[14] I. Lobach, S. Nagaitsev, V. Lebedev, A. Romanov, G. Stancari, A. Valishev et al., *Measurements of undulator radiation power noise and comparison with ab initio calculations*, *Phys. Rev. Accel. Beams* **24** (2021) 040701 [arXiv:2012.00965].

[15] V. Lebedev, J. Jarvis, H. Piekarz, A. Romanov, J. Ruan and M. Andorf, *Conceptual Design Report: Optical Stochastic Cooling at IOTA*, Tech. Rep., FERMILAB-PUB-20-656-AD, Fermilab (2020) arXiv:2012.09967.

[16] G. Stancari, *Detecting single electrons in IOTA*, talk presented at the *Workshop on Single-Electron Experiments in IOTA*, Fermilab, 9 November 2018, https://indico.fnal.gov/event/18395/contributions/46977.

[17] A. Romanov, J. Santucci, G. Stancari, A. Valishev and N. Kuklev, *Experimental 3-dimensional tracking of the dynamics of a single electron in the Fermilab Integrable Optics Test Accelerator (IOTA)*, arXiv:2012.04148.

[18] *IOTA/FAST Scientific Committee (ISC) Web page*, https://cdcvs.fnal.gov/redmine/projects/ifsc/wiki.

2021 JINST 16 P05002

[19] V. Shiltsev, Y. Alexahin, V. Kamerdzhiev, G. Kuznetsov, X.-L. Zhang and K. Bishofberger, *Experimental Demonstration of Compensation of Beam-Beam Effects by Electron Lenses*, *Phys. Rev. Lett.* **99** (2007) 244801 [arXiv:0705.0320].

[20] V. Shiltsev et al., *Tevatron Electron Lenses: Design and Operation*, *Phys. Rev. ST Accel. Beams* **11** (2008) 103501 [arXiv:0808.1542].

[21] X.-L. Zhang, K. Bishofberger, V. Kamerdzhiev, V. Lebedev, V. Shiltsev, R. Thurman-Keup et al., *The Origination and Diagnostics of Uncaptured Beam in the Tevatron and Its Control by Electron Lenses*, *Phys. Rev. ST Accel. Beams* **11** (2008) 051002 [arXiv:0804.2407].

[22] G. Stancari, A. Valishev, G. Annala, G. Kuznetsov, V. Shiltsev, D.A. Still et al., *Collimation with hollow electron beams*, *Phys. Rev. Lett.* **107** (2011) 084802 [arXiv:1105.3256].

[23] W. Fischer et al., *Operational Head-on Beam-Beam Compensation with Electron Lenses in the Relativistic Heavy Ion Collider*, *Phys. Rev. Lett.* **115** (2015) 264801.

[24] I. Béjar Alonso, O. Brüning, P. Fessia, M. Lamont, L. Rossi, L. Tavian et al., eds., *High-Luminosity Large Hadron Collider (HL-LHC): Technical Design Report*, CERN Yellow Reports: Monographs, CERN, Geneva, Switzerland (2020), DOI: 10.23731/CYRM-2020-0010.

[25] G. Stancari, V. Previtali, A. Valishev, R. Bruce, S. Redaelli, A. Rossi et al., *Conceptual design of hollow electron lenses for beam halo control in the Large Hadron Collider*, Tech. Rep., FERMILAB-TM-2572-APC, Fermilab (2014).

[26] D. Perini, G. Gobbi, D.J. Crawford, J. Ruan, G. Stancari, L.R. Valerio et al., *The development programme of cathodes and electron guns for the hollow electron lenses of the High Luminosity LHC Project*, in *Proceedings of the 10th International Particle Accelerator Conference*, Melbourne, Australia, 19–24 May 2019, pp. 1102–1105 [FERMILAB-CONF-19-337-AD].

[27] X. Gu et al., *Halo removal experiments with hollow electron lens in the BNL Relativistic Heavy Ion Collider*, *Phys. Rev. Accel. Beams* **23** (2020) 031001.

[28] M. Fitterer, G. Stancari, A. Valishev, S. Redaelli and D. Valuch, *Resonant and random excitations on the proton beam in the Large Hadron Collider for active halo control with pulsed hollow electron lenses*, *Phys. Rev. Accel. Beams* **24** (2021) 021001 [arXiv:1804.07418].

[29] S. Redaelli et al., *Hollow electron lenses for beam collimation at the High-Luminosity Large Hadron Collider (HL-LHC)*, 2021 *JINST* **16** P03042.

[30] D. Mirarchi, R.B. Appleby, R. Bruce, G. Giovannozzi, A. Mereghetti, S. Redaelli et al., *Nonlinear dynamics of proton beams with hollow electron lens in the CERN High-Luminosity LHC*, submitted to *Eur. Phys. J. Plus* (2021).

[31] S. Artikova, O. Boine-Frankenheim, O. Meusel, A. Oeftiger, D. Ondreka, K. Schulte-Urlichs et al., *Pulsed electron lenses for space charge compensation in the FAIR synchrotrons*, 2021 *JINST* **16** P03044.

[32] V.D. Shiltsev, *Electron Lenses for Super-Colliders*, Springer (2016), DOI: 10.1007/978-1-4939-3317-4.

[33] V.V. Danilov and V.D. Shiltsev, *"Round colliding beams" as a way to integrability: Theory and simulations for Tevatron*, Tech. Rep., FERMILAB-FN-655, Fermilab (1997).

[34] V.V. Danilov and V.D. Shiltsev, *On possibility of footprint compression with one lens in nonlinear accelerator lattice*, Tech. Rep., FERMILAB-FN-671, Fermilab (1998).

2021 JINST 16 P05002

[35] V. Danilov and V. Shiltsev, *On the possibility of footprint compression with one lens in nonlinear accelerator lattice*, 2021 *JINST* **16** P03050.

[36] S. Nagaitsev and T. Zolkin, *Betatron frequency and the Poincaré rotation number*, *Phys. Rev. Accel. Beams* **23** (2020) 054001 [arXiv:1910.08630].

[37] E.M. McMillan, *Some thoughts on stability in nonlinear periodic focusing systems*, Tech. Rep., UCRL-17795, Lawrence Radiation Laboratory, University of California, Berkeley, California (1967).

[38] E.M. McMillan, *A problem in the stability of periodic systems*, in *Topics in Modern Physics: A Tribute to Edward U. Condon*, W.E. Brittin and H. Odabasi, eds., pp. 219–244, Colorado Associated University Press, Boulder, CO, U.S.A. (1971).

[39] B. Cathey, G. Stancari, A. Valishev and T. Zolkin, *Calculations of detuning with amplitude for the McMillan electron lens in the Fermilab Integrable Optics Test Accelerator (IOTA)*, 2021 *JINST* **16** P03041.

[40] G. Stancari, A. Burov, V. Lebedev, S. Nagaitsev, E. Prebys and A. Valishev, *Electron lenses and cooling for the Fermilab Integrable Optics Test Accelerator*, in *Proceedings of the International Workshop on Beam Cooling and Related Topics*, Newport News, Virginia, U.S.A., 28 September–2 October 2015, pp. 32–35 [arXiv:1511.01812].

[41] H. Poth, *Electron cooling: Theory, experiment, application*, *Phys. Rept.* **196** (1990) 135.

[42] G. Tranquille et al., *Commissioning the ELENA beam diagnostics systems at CERN*, in *Proceedings of the 9th International Particle Accelerator Conference*, Vancouver, Canada, 29 April–4 May 2018, pp. 2043–2046.

[43] L.D. Landau, *On the vibrations of the electronic plasma*, *J. Phys. (USSR)* **10** (1946) 25.

[44] J.S. Berg and F. Ruggiero, *Landau damping with two-dimensional betatron tune spread*, Tech. Rep., CERN-SL-96-071-AP, CERN, Geneva (1996).

[45] A. Burov, *Nested Head-Tail Vlasov Solver*, *Phys. Rev. ST Accel. Beams* **17** (2014) 021007 [arXiv:1309.0044].

[46] R. Tomás et al., *FCC study: parameters and optics for hadron and lepton colliders*, *Nucl. Part. Phys. Proc.* **273-275** (2016) 149.

[47] M. Benedikt and F. Zimmermann, *Towards future circular colliders*, *J. Korean Phys. Soc.* **69** (2016) 893.

[48] D. Schulte, *FCC-hh layout and parameters*, talk presented at the *3rd Annual Meeting of the Future Collider Study*, Berlin, Germany, 29 May–2 June 2017, https://indico.cern.ch/event/556692/contributions/2484245/.

[49] W. Scandale, *Dynamic aperture*, *AIP Conf. Proc.* **326** (1995) 52.

[50] V. Shiltsev, Y. Alexahin, A. Burov and A. Valishev, *Landau Damping of Beam Instabilities by Electron Lenses*, *Phys. Rev. Lett.* **119** (2017) 134802 [arXiv:1706.08477].

[51] O. Boine-Frankenheim and W.D. Stem, *Space charge compensation with pulsed electron lenses for intense ion beams in synchrotrons*, *Nucl. Instrum. Meth. A* **896** (2018) 122 [arXiv:1705.01057].

[52] R. Ainsworth, *Ensuring bunch stability in multi-MW beams*, Department of Energy Early Career Research Program for Fiscal Year 2020, https://science.osti.gov/-/media/early-career/pdf/FY20_DOE_SC_Early_Career_Research_Program_Abstracts.pdf?la=en&hash=14F446091C8D06C3AC9E0BF347243173F00F75D6, 2020.

2021 JINST 16 P05002

[53] A. Burov, G.W. Foster and V.E. Shiltsev, *Space-charge compensation in high-intensity proton rings*, Tech. Rep., FNAL-TM-2125, Fermilab (2000).

[54] Y. Alexahin, A. Drozhdin, N. Kazarinov and X. Yang, *Effects of space charge and magnet nonlinearities on beam dynamics in the Fermilab Booster*, in *Proceedings of the 22nd Particle Accelerator Conference*, Albuquerque, New Mexico, U.S.A., 25–29 June 2007, pp. 3474–3476.

[55] Y. Alexahin and V. Kapin, *Study of possibility of space charge compensation in the Fermilab Booster with multiple electron columns*, Tech. Rep., Beams-doc-3108, Fermilab (2008).

[56] Y. Alexahin and V. Kapin, *On possibility of space-charge compensation in the Fermilab Booster with multiple electron columns*, 2021 *JINST* **16** P03049.

[57] V.N. Litvinenko and G. Wang, *Compensating tune spread induced by space charge in bunched beams*, *Phys. Rev. ST Accel. Beams* **17** (2014) 114401 [arXiv:1405.2352].

[58] D. Ondreka, P. Spiller, P. Apse-Apsitis and K. Schulte, *Overcoming the space charge limit: Development of an electron lens for SIS18*, in *Proceedings of the 8th International Particle Accelerator Conference*, Copenhagen, Denmark, 14–19 May 2017, pp. 2211–2213.

[59] E. Stern, *PIC simulations of space charge compensation with electron lens*, Tech. Rep., Beams-doc-7567, Fermilab (2019).

[60] E. Stern, Y. Alexahin, A. Burov and V. Shiltsev, *Self-consistent PIC Simulations of Ultimate Space Charge Compensation with Electron Lenses.*, 2021 *JINST* **16** P03045.

[61] J.S. DeGrassie and J.H. Malmberg, *Wave-induced transport in the pure electron plasma*, *Phys. Rev. Lett.* **39** (1977) 1077.

[62] D.H.E. Dubin and T.M. O'Neil, *Trapped nonneutral plasmas, liquids, and crystals (the thermal equilibrium states)*, *Rev. Mod. Phys.* **71** (1999) 87.

[63] V.D. Shiltsev, *On possibility to compensate space charge effects by controlled electron columns*, Tech. Rep., FNAL-Beams-doc-2810-v1, Fermilab (2007).

[64] V.D. Shiltsev, *New possibilities for beam-beam and space-charge compensation: MCP gun and electron columns*, in *Proceedings of the 22nd Particle Accelerator Conference*, Albuquerque, New Mexico, U.S.A., 25–29 June 2007, pp. 1159–1160 [https://accelconf.web.cern.ch/p07/PAPERS/TUPMN106.PDF].

[65] G.I. Budker, G.I. Dimov, V.G. Dudnikov, A.A. Sokolov and V.G. Shamovsky, *Experiments on electron compensation of proton beam in ring accelerator*, in *Proceedings of the 6th International Conference on High-Energy Accelerators*, Cambridge, Massachusetts, U.S.A., 11–15 September 1967 pp. A103–A105 [https://inspirehep.net/literature/921150].

[66] Y.I. Belchenko, G.I. Budker, G.E. Derevyankin, G.I. Dimov, V.G. Dunikov, G.V. Roslyakov et al., *High current proton beams at Novosibirsk*, in *Proceedings of the 10th International Conference on High-Energy Accelerators*, Protvino, USSR, 11–17 July 1977, pp. 287–294 [https://inspirehep.net/literature/127164].

[67] Y.I. Belchenko, *High current proton beams at Novosibirsk: Electron compensation, charge exchange injection, negative ion sources*, Tech. Rep., LA-TR-78-53, CONF-770709-23, Fermilab (1978).

[68] G.I. Dimov and V.E. Chupriyanov, *Compensated proton-beam production in an accelerating ring at a current above the space-charge limit*, *Part. Accel.* **14** (1984) 155.

[69] V. Dudnikov, *Condition for Production of Circulating Proton Beam with Intensity Greater than Space Charge Limit*, *AIP Conf. Proc.* **642** (2002) 367.

2021 JINST 16 P05002

[70] V.D. Shiltsev, A. Valishev, G. Kuznetsov, V. Kamerdzhiev and A. Romanov, *Beam studies with electron columns*, in *Proceedings of the 23rd Particle Accelerator Conference*, Vancouver, BC, Canada, 4–8 May 2009, pp. 3233–3235 [https://accelconf.web.cern.ch/pac2009/papers/th5pfp020.pdf].

[71] R.E. Pollock, J. Ellsworth, M.W. Muterspaugh and D.S. Todd, *Proton beam-electron plasma interactions*, *AIP Conf. Proc.* **498** (1999) 336.

[72] D.S. Todd and R.E. Pollock, *An experiment to transfer angular momentum from a helical low energy proton beam to a trapped electron plasma*, *AIP Conf. Proc.* **606** (2002) 223.

[73] M.E. Rudd, Y.K. Kim, D.H. Madison and J.W. Gallagher, *Electron production in proton collisions: total cross sections*, *Rev. Mod. Phys.* **57** (1985) 965.

[74] M. Chung, L. Prost and V.D. Shiltsev, *Space-charge compensation for high-intensity linear and circular accelerators at fermilab*, in *Proceedings of the 2013 North American Particle Accelerator Conference*, Pasadena, CA, U.S.A., 29 September– 4October 2013, pp. 402–404 [https://accelconf.web.cern.ch/pac2013/papers/tuobb1.pdf].

[75] C.S. Park, V.D. Shiltsev, G. Stancari, J.C.T. Thangaraj and D. Milana, *Space charge compensation using electron columns and electron lenses at IOTA*, in *Proceedings of the 2016 North American Particle Accelerator Conference*, Chicago, IL, U.S.A., 9–14 October 2016, pp. 1257–1259.

[76] B.T. Freemire, S. Chattopadhyay, V.D. Shiltsev, G. Stancari, C.S. Park, G. Penn et al., *Simulations of the electron column in IOTA*, in *Proceedings of the 9th International Particle Accelerator Conference*, Vancouver, BC, Canada, April 29–May 4 2018, pp. 1103–1106.

[77] B.T. Freemire, S. Chattopadhyay, V.D. Shiltsev, G. Stancari, C.S. Park, G. Penn et al., *Space-charge compensation using electron columns at IOTA*, in *Proceedings of the 61st Advanced Beam Dynamics Workshop on High-Intensity and High-Brightness Hadron Beams*, Daejeon, South Korea, 17–22 June 2018, pp. 247–251.

[78] B.T. Freemire, S. Chattopadhyay, E.G. Stern, C.S. Park, C.E. Mitchell, R.D. Ryne et al., *Multipass simulations of space charge compensation using an electron column at IOTA*, in *Proceedings of the 10th International Particle Accelerator Conference*, Melbourne, Australia, 19–24 May 2019, pp. 3313–3316.

[79] A. Friedman et al., *Computational methods in the Warp code framework for kinetic simulations of particle beams and plasmas*, *IEEE Trans. Plasma Sci.* **42** (2014) 1321.

[80] *Warp*, http://warp.lbl.gov.

[81] J. Amundson, P. Spentzouris, J. Qiang and R. Ryne, *Synergia: An accelerator modeling tool with 3-D space charge*, *J. Comp. Phys.* **211** (2006) 229.

[82] *Synergia*, https://synergia.fnal.gov.

[83] C.S. Park, B. Freemire, M. Chung, G. Stancari and E. Stern, *Progress in space charge compensation using electron columns*, 2021 *JINST* **16** P03048.

[84] A. Kalimov, C. Muehle, D. Ondreka, K. Schulte-Urlichs and P. Spiller, *Optimization of a solenoid for an electron lens in SIS18*, *IEEE Trans. Appl. Supercond.* **30** (2020) 1.

[85] Y. Alexahin, A. Burov and V. Shiltsev, *Landau damping with electron lenses in space-charge dominated beams*, Tech. Rep., FERMILAB-TM-2655-APC, Fermilab (2017).

[86] Y. Alexahin, A. Burov and V. Shiltsev, *Landau Damping with Electron Lenses in Space-Charge Dominated Beams*, 2021 *JINST* **16** P03046.

2021 JINST 16 P05002

[87] A.V. Burov, V. Danilov and V. Shiltsev, *Transverse beam stability with an "electron lens"*, *Phys. Rev. E* **59** (1999) 3605.

[88] I. Lobach, S. Nagaitsev, E. Stern and T. Zolkin, *McMillan lens in a system with space charge*, in *Proceedings of the 9th International Particle Accelerator Conference*, Vancouver, BC, Canada, April 29–May 4 2018, pp. 3143–3145.

[89] S. Nagaitsev, I. Lobach, E. Stern and T. Zolkin, *McMillan electron lens in a system with space charge*, 2021 *JINST* **16** P03047.

[90] R.C. Dhuley, C. Boffo, V. Kashikhin, A. Kolehmainen, D. Perini and G. Stancari, *Design of a compact, cryogen-free superconducting solenoid for the electron lens of the Fermilab Integrable Optics Test Accelerator (IOTA)*, 2021 *JINST* **16** T03009.

[91] D.A. Edwards and L.C. Teng, *Parametrization of linear coupled motion in periodic systems*, *IEEE Trans. Nucl. Sci.* **20** (1973) 885.

[92] F. Willeke and G. Ripken, *Methods of Beam Optics*, *AIP Conf. Proc.* **184** (2008) 758.

[93] V.A. Lebedev and S.A. Bogacz, *Betatron Motion with Coupling of Horizontal and Vertical Degrees of Freedom*, 2010 *JINST* **5** P10010 [arXiv:1207.5526].

[94] L. Deniau, H. Grote, G. Roy and F. Schmidt, *MAD – Methodical Accelerator Design*, http://mad.web.cern.ch/mad.

[95] A.V. Burov, *Electron drift instability in storage rings with electron cooling*, *Nucl. Instrum. Meth. A* **441** (2000) 23.

[96] A. Burov, *Two-Beam Instability in Electron Cooling*, *Phys. Rev. ST Accel. Beams* **9** (2006) 120101.

[97] Y.H. Jo, J.S. Kim, G. Stancari, M. Chung and H.J. Lee, *Control of the diocotron instability of a hollow electron beam with periodic dipole magnets*, *Phys. Plasmas* **25** (2017) 011607.

[98] G. Stancari, *Electron-beam simulations: Electron-gun emission and residual fields from measured profiles*, talk presented at the *CERN Meeting on Hollow Electron Lens Beam Results*, CERN, 26 January 2018, https://indico.cern.ch/event/698949/contributions/2868279.

[99] R.C. Davidson, *Physics of Nonneutral Plasmas*, World Scientific (2001).

[100] D. Noll and G. Stancari, *Field calculations, single-particle tracking, and beam dynamics with space charge in the electron lens for the Fermilab Integrable Optics Test Accelerator*, Tech. Rep., FERMILAB-TM-2598-AD-APC, Fermilab (2015) [DOI: 10.2172/1230044].

[101] D. Noll, M. Droba, O. Meusel, U. Ratzinger, K. Schulte and C. Wiesner, *The particle-in-cell code bender and its application to non-relativistic beam transport*, in *Proceedings of the 54th ICFA Advanced Beam Dynamics Workshop on High Intensity, High Brightness and High Power Hadron Beams*, East Lansing, MI, U.S.A., 10–14 November 2014, pp. 304–308, [http://accelconf.web.cern.ch/HB2014/papers/weo4lr02.pdf].

[102] *COMSOL Multiphysics*, https://www.comsol.com.

[103] *CST Studio Suite*, Dassault Systèmes, https://www.3ds.com.

[104] R. Dhuley, *Cooldown analysis of the IOTA electron-lens superconducting magnet with cryocooler conduction cooling*, Tech. Rep., FERMILAB-TM-2738-AD-TD, Fermilab (2020).

[105] D. Perini, A. Kolhemainen, A. Rossi, S. Sadovich and G. Stancari, *Design of high-performance guns for the HL-LHC HEL*, 2021 *JINST* **16** T03010.

2021 JINST 16 P05002

[106] A.N. Sharapa and A.V. Shemyakin, *Electron cooling device without bending magnets*, *Nucl. Instrum. Meth. A* **336** (1993) 6.

[107] V.M. Barbashin, *Prototype of an electron cooling device without bending magnets*, *Nucl. Instrum. Meth. A* **366** (1995) 215.

[108] G. Ciullo, A.N. Sharapa, A.V. Shemyakin and L. Tecchio, *Characteristics of the beams generated by a 'hollow cathode' electron gun*, *Rev. Sci. Instrum.* **69** (1998) 59.

[109] X. Gu et al., *The electron lens test bench for the relativistic heavy ion collider at Brookhaven National Laboratory*, *Nucl. Instrum. Meth. A* **743** (2014) 56.

[110] X. Gu et al., *Transverse profile of the electron beam for the RHIC electron lenses*, *Nucl. Instrum. Meth. A* **798** (2015) 36.

[111] R.E. Pollock and F. Anderegg, *Spin-up of an electron plasma — first results*, *AIP Conf. Proc.* **331** (1995) 139.

[112] E.M. Hollmann, F. Anderegg and C.F. Driscoll, *Confinement and manipulation of non-neutral plasmas using rotating wall electric fields*, *Phys. Plasmas* **7** (2000) 2776.

[113] S. Szustkowski, S. Chattopadhyay, D.J. Crawford and B.T. Freemire, *Skimmer-nozzle configuration measurements for a gas sheet beam profile monitor*, in *Proceedings of the North American Particle Accelerator Conference*, Lansing, Michigan, U.S.A., 2–6 September 2019, pp. 573–575.

[114] J. Eldred, V. Lebedev, K. Seiya and V. Shiltsev, *Studies of beam intensity effects in Fermilab Booster synchrotron*, Tech. Rep., FERMILAB-PUB-20-673-AD-APC, Fermilab (2020).

[115] J. Eldred, V. Lebedev, K. Seiya and V. Shiltsev, *Beam intensity effects in Fermilab Booster synchrotron*, *Phys. Rev. Accel. Beams* **24** (2021) 044001 [arXiv:2012.12255].

[116] V. Shiltsev, *Space-charge effects in ionization beam profile monitors*, *Nucl. Instrum. Meth. A* **986** (2021) 164744.

[117] C. Xu, B. Dehning, F.S. Domingues Sousa and E. Griesmayer, *Diamond monitor based beam loss measurements in the LHC*, in *Proceedings of the 5th International Beam Instrumentation Conference*, Barcelona, Spain, 11–15 September 2016, pp. 82–85.

[118] A.A. Warner, *Thin sCVD diamond halo/loss monitor*, Fermilab Lab Directed Research and Development (LDRD) Proposal (unpublished), 2015.

[119] C. Rubbia, *Microwave radiation from the transverse temperature of an intense electron beam confined by a longitudinal magnetic field*, Tech. Rep., CERN-EP-77-4, CERN, Geneva, Switzerland (1977).

[120] J. Bridges, J. Gannon, E.R. Gray, J. Griffin, F.R. Huson, D.E. Johnson et al., *Fermilab electron cooling experiment: Design report*, Tech. Rep., FERMILAB-DESIGN-1978-01, Fermilab, Batavia IL, U.S.A. (1978), DOI 10.2172/1155428.

[121] G. Tranquille, *Diagnostics for electron cooled beams*, in *Proceedings of the European Workshop on Beam Diagnostics and Instrumentation for Particle Accelerators*, Mainz, Germany, 5–7 May 2003, pp. 110–112, [http://accelconf.web.cern.ch/AccelConf/d03/papers/PM09.pdf] [CERN-AB-2003-059-BDI].

[122] R.W. Gould and M.A. LaPointe, *Cyclotron resonance in a pure electron plasma column*, *Phys. Rev. Lett.* **67** (1991) 3685.

[123] N.C. Luhmann, H. Bindslev, H. Park, J. Sánchez, G. Taylor and C.X. Yu, *Chapter 3: Microwave diagnostics*, *Fusion Sci. Technol.* **53** (2008) 335.

2021 JINST 16 P05002

[124] Project 8 collaboration, *Single electron detection and spectroscopy via relativistic cyclotron radiation*, *Phys. Rev. Lett.* **114** (2015) 162501 [arXiv:1408.5362].

[125] C. Crawford, F. Niell, G. Saewert, J. Santucci, A. Sery, A. Shemyakin et al., *Prototype "electron lens" set-up for the Tevatron beam-beam compensation*, in *Proceedings of the 1999 Particle Accelerator Conference*, New York City, NY, U.S.A., 29 March–2 April 1999, vol. 1, pp. 237–239.

[126] C. Crawford, A. Sery, V. Shiltsev, A. Aleksandrov, B. Skarbo and B. Sukhina, *Magnetic field alignment in the beam-beam compensation device*, in *Proceedings of the 1999 Particle Accelerator Conference*, New York City, NY, U.S.A., 29 March–2 April 1999, vol. 5, pp. 3321–3323.

2021 JINST 16 P05002